

Accelerator Based Epithermal Neutron Source

S. Yu. Taskaev

Budker Institute of Nuclear Physics, pr. Lavrentieva 11, Novosibirsk, 630090 Russia

Novosibirsk State University, ul. Pirogova 2, Novosibirsk, 630090 Russia

e-mail: taskaev@inp.nsk.su

Abstract—We review the current status of the development of accelerator sources of epithermal neutrons for boron neutron capture therapy (BNCT), a promising method of malignant tumor treatment. Particular attention is given to the source of epithermal neutrons on the basis of a new type of charged particle accelerator: tandem accelerator with vacuum insulation and lithium neutron-producing target. It is also shown that the accelerator with specialized targets makes it possible to generate fast and monoenergetic neutrons, resonance and monoenergetic gamma-rays, alpha-particles, and positrons.

DOI: 10.1134/S1063779615060064

INTRODUCTION

According to the World Health Organization, cancer incidence has been steadily increasing and leads to significant mortality. Drug development and treatment of malignant tumors is an important and hitherto not solved scientific problem. Boron-neutron capture therapy (BNCT) is a promising approach in the treatment of a variety of malignant tumors, especially intractable brain tumors, exerting extremely effective selective impact directly on cancer cells.

BNCT is a binary form of radiation therapy that uses a unique high ability of non-radioactive boron-10 nucleus to absorb thermal neutrons. The cross section of this absorption reaction is 3837 b. The absorption of the neutron by the ^{10}B nucleus leads to an instant

nuclear reaction $^{10}\text{B}(n,\alpha)^7\text{Li}$ with an energy release of 2.79 MeV. In 6.1% cases, the energy is distributed only between the nuclei of lithium and α -particles, in 93.9% of cases the lithium nucleus is emitted in an excited state and emits a γ -quantum with an energy of 0.48 MeV (Fig. 1). The products of the nuclear reaction, namely the nucleus of lithium with an energy of 0.84 MeV and α -particle with an energy of 1.47 MeV, are characterized by high stopping power (averages 162 and 196 $\text{keV } \mu\text{m}^{-1}$, respectively) and a small range of these particles in water or in the body tissues—5.2 and 7.5 microns, respectively (the size of typical mammalian cell). The stopping power of γ -quantum is significantly lower—0.3 $\text{keV } \mu\text{m}^{-1}$. Therefore, the main part of the energy release in the nuclear reaction

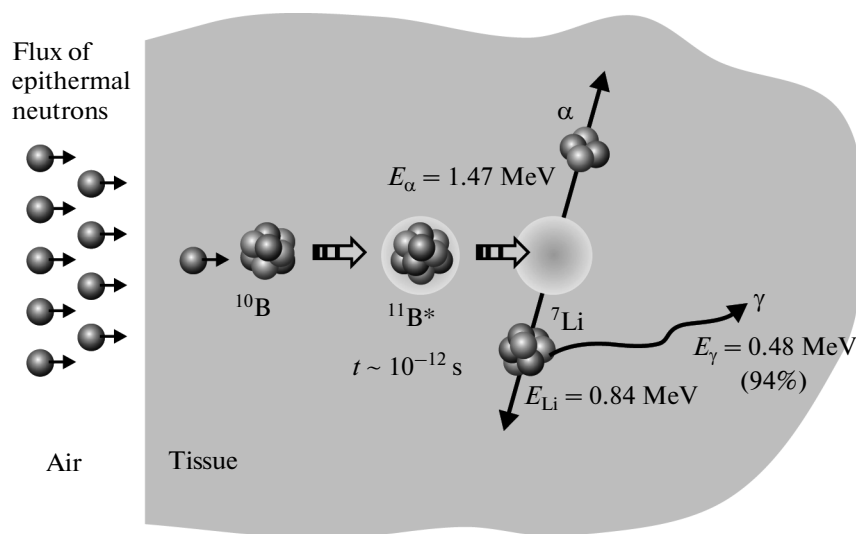


Fig. 1. Schematic representation of the BNCT principle.

$^{10}\text{B}(n,\alpha)^7\text{Li}$, namely 84%, occurs within a single cell. Therefore, selective accumulation of boron-10 in the tumor cells and subsequent irradiation with neutrons should lead to the destruction of tumor cells with relatively little damage to the surrounding normal cells. This basic idea of BNCT was formulated by Locher in 1936 [1], soon after the discovery of the neutron by Chadwick [2] and the description of Taylor and Goldhaber the reaction $^{10}\text{B}(n,\alpha)^7\text{Li}$ [3].

The first neutron irradiation of tumor fragments with boric acid was conducted in 1940 by Kruger [4]. In 1951, an important result was obtained by Sweet—selective accumulation of boron in the tumor cells of the patient was established [5, 6]. From that time a clinical application of BNCT has began.

In accordance with the introductory article by Sauerwein in a recent book on the neutron capture therapy [7, p. 3], one can discriminate four periods in the development of the BNCT technique.

The first period is associated with early clinical trials conducted in the United States from 1951 to 1961 on nuclear reactors in Brookhaven and at MIT [8, 9]. These tests did not show therapeutic efficacy of the used method in [10, 11]. The reason had to do with a poor selectivity and low concentration of boron, due to which a “background” radiation with recoil protons and γ -rays as a result of reactions $^{14}\text{N}(n,p)^{14}\text{C}$ and $^1\text{H}(n,\gamma)^2\text{H}$ was relatively large.

The second period is associated with the pioneering works by Hatanaka and co-workers, held in Japan from 1968 to the end of the 1980s. Hatanaka began to apply an intra-arterial injection of borocaptate sodium (BSH, $\text{Na}_2\text{B}_{12}\text{H}_{11}\text{SH}$) enriched by the ^{10}B isotope, synthesized by Solovay [12]. He conducted an open exposure of the tumor after surgery and has achieved impressive results: the 5-year survival rate was 58% for the group of patients with malignant gliomas of grades 3 and 4 [13]. In 1987, Mishima carried out the surface treatment of malignant melanoma, using the boronphenylealanine enriched by the ^{10}B isotope in optically isomeric form L (BPA, $(\text{HO})_2^{10}\text{B}-\text{C}_6\text{H}_4-\text{CH}_2\text{CH}(\text{NH}_2)-\text{CO}_2\text{H}$) [14].

These results gave the impetus to the third period of the neutron capture therapy: clinical trials of deep intracerebral tumors using epithermal neutron beams from nuclear reactors. The therapy of patients was conducted in Brookhaven [15] and Cambridge [16] in the US, in the Netherlands [17], Finland [18], Sweden [19], Czech Republic [20], Japan [21], Argentina [22], and Taiwan [23]. BNCT has been extended to other diseases, such as the neck malignant tumor [24, 25], meningioma [26], pleural mesothelioma [27], and hepatocellular carcinoma [28]. Despite the efforts and scientific progress, internal problems led to a serious crisis. Until now, only the nuclear reactors were able to produce the required epithermal neutron beams. However, the functioning of these systems is highly

dependent on policy support, and for various reasons they discontinued the therapy conducting, except the THOR reactor (Taiwan) and the nuclear center at Bariloche (Argentina). All these actions were only caused because of political and economic reasons, and not clinical outcomes. Currently, research on BNCT inevitably trigger a new period associated with the use of particle accelerators to produce the beams of epithermal neutrons. The first discussions and suggestions to design accelerator BNCT sources fall at the end of the 1980s to the early 1990s, as a result of the progress reached in the methodology of clinical trials at nuclear reactors. This subject is currently of particular relevance due to the closure of almost all the nuclear reactors used for clinical trials of BNCT. Of additional importance to the concept of BNCT accelerator is the fact that the resulting neutron beams can provide a better quality of therapy than the nuclear reactor beams. Over the past 25 years numerous projects of accelerator neutron sources were proposed, but because of the complexity of the problem quite a small number of them can be implemented in the near future.

The main requirement for the therapeutic beam of neutrons is often the following: the flux of epithermal neutrons has to be higher than $10^9 \text{ cm}^{-2} \text{ s}^{-1}$, so that the duration of therapy would be shorter than an hour. Epithermal neutrons are those having the energies in the range from 0.5 to 10 keV. Using epithermal neutrons is caused by the necessity to maximize the density of thermal neutrons at the depth of location of the tumor. In the therapeutic beam, the flows of slow neutrons, fast neutrons, and γ -rays can be present. Slow neutrons lead to higher non-localized dose as a result of absorption by nitrogen and hydrogen with emission of a proton and γ -quantum, respectively. Elastic scattering of fast neutrons on nuclei (mostly hydrogen) leads to the formation of the recoil protons and makes a significant contribution to the dose at the surface. Since it is impossible to completely get rid of fast neutrons and γ -radiation, it is recommended to limit their contributions to a dose magnitude of $2 \times 10^{-13} \text{ Gy}$ per one epithermal neutron. These requirements were formulated after analyzing the results of clinical testing of methodology, conducted on nuclear reactors and formulating the recommendations for accelerator neutron sources.

Over the last decade a significant progress has been achieved in development of the accelerating concept of BNCT, particularly in optimization of beam shaping assembly, and there is a better understanding of what is required. It became clear that the term “epithermal neutrons” needs to be clarified. There is a too wide range of neutron energies, so that they all could not be optimized for BNCT. This awareness was reflected in recently published book on the neutron capture therapy. In the chapter on accelerators, A. Kreiner repeats the statement of the need for using

epithermal neutrons, but specifies that “the perfect spectrum corresponds to the range centered near the top of the range,” i.e., 10 keV [7, p. 43]. In the next chapter of the same book, Leung makes a similar statement but in somewhat different words: ideal for BNCT are the neutrons with energies from 1 to 30 keV [7, Fig. 4.11 at p. 65].

The spectrum and neutron flux density by themselves are not the ultimate goals of research. For therapy, the important values are the dose, the therapeutic ratio and the depth of therapy, which depend not only on the beam parameters but also on the concentration of boron in the tumor and normal tissues. It is these parameters which can determine the quality of treatment. Therapeutic ratio (advantage ratio AR) is the ratio of the maximum dose rate in tumor and in normal tissues. The depth of therapy (advantage depth AD) is called the distance between the irradiated surface and the tumor in which the dose exceeds the maximum dose for normal tissues in the bulk. Neutron beams from nuclear reactors could produce a dose rate of 0.2–2 Gy/min, a therapeutic ratio of 4–6 and a depth of therapy from 8 to 9.7 cm with boron concentration of 18 and 65 ppm, respectively, in normal tissues and tumors [7, p. 30]. Thus, the requirement to the accelerator neutron sources is formulated as follows: the dose should be at least 1 Gy/min, the depth of treatment not less than 8 cm, and a therapeutic ratio of at least 4.

The paper presents an overview of accelerator neutron sources for BNCT and the details of studies on the development of a neutron source in BINP based on an original tandem accelerator with vacuum insulation. At the end of the review we briefly discuss possible applications of the accelerator for other purposes.

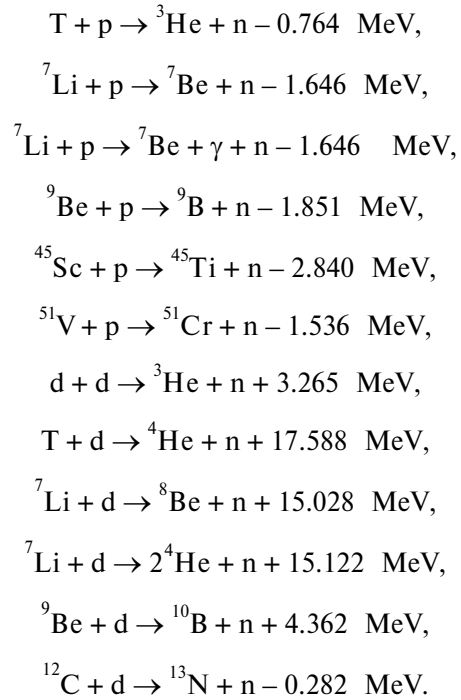
NEUTRON EMISSION REACTIONS

In clinical trials of BNCT, nuclear reactors are used as the neutron sources. In these reactors, the reaction of ^{235}U fission is used and induced by thermal neutrons. The energy spectrum of neutrons emitted is well described by the distribution $F(E) = 0.77\sqrt{E}\exp(-0.775E)$ [7, p. 43]. The spectrum extends to 10 MeV, and has a mean energy of around 2 MeV. During BNCT, neutron moderation is performed using a beam shaping assembly comprising the moderator, reflector, absorber, and filters.

For obtaining neutrons by means of the beams of charged particles, nuclear reactions involving the nuclei with loosely bound neutrons are commonly used. There are two types of reactions from the energetic point of view. Exothermic reactions require a minimum kinetic energy of particles. A typical example is the d-d reaction, as a result of which the neutron and tritium are formed. The energy yield of this reac-

tion is 3.265 MeV. This means that the neutron formed has an energy of 2.451 MeV when the energy of deuteron is neglected and a higher energy if this energy is taken into account. One can see that the neutron energy is even greater than the mean energy of neutron in the nuclear fission reaction. Another type of reaction is called endothermic and it requires minimal threshold energy of particles. Near the threshold the neutron energy is very small, so that the use of neutrons for BNCT is very effective.

The main reactions of the neutron generation are the following [29]:



Figures 2 and 3 show the cross sections of the main reactions [30]. The neutron yield is shown in Fig. 4, and the main parameters of these reactions are presented in Table 1 [31, 32].

In [31] it has been noted that the most attention is being focused on the following four reactions: ${}^7\text{Li}(p,n){}^7\text{Be}$, ${}^9\text{Be}(p,n){}^9\text{B}$, ${}^9\text{Be}(d,n){}^{10}\text{B}$, and ${}^{12}\text{C}(d,n){}^{14}\text{N}$. The best of these reactions was recognized as the reaction ${}^7\text{Li}(p,n){}^7\text{Be}$ due to the maximum yield and minimum energy of neutrons. However, creating lithium target seemed to be problematic due to a low melting temperature, low thermal conductivity, high chemical reactivity of lithium, and because of production of ${}^7\text{Be}$ radioactive isotope. After 10 years, A. Kreiner in his review on accelerator neutron sources emphasizes [7] that only three reactions providing the generation of neutrons with energies lower than that obtained in the nuclear reactors should be considered. This concerns the threshold reactions ${}^7\text{Li}(p,n){}^7\text{Be}$, ${}^9\text{Be}(p,n){}^9\text{B}$, and ${}^{12}\text{C}(d,n){}^{13}\text{N}$. The last of these reactions is actually not considered due to the low yield of neutrons. Of the

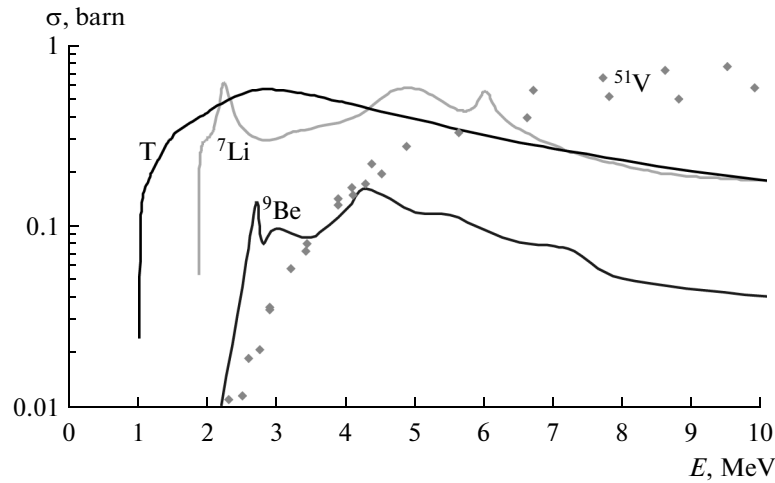


Fig. 2. The cross section of neutron generation in the interaction of a proton beam with the target of tritium, lithium-7, beryllium-9, and vanadium-51.

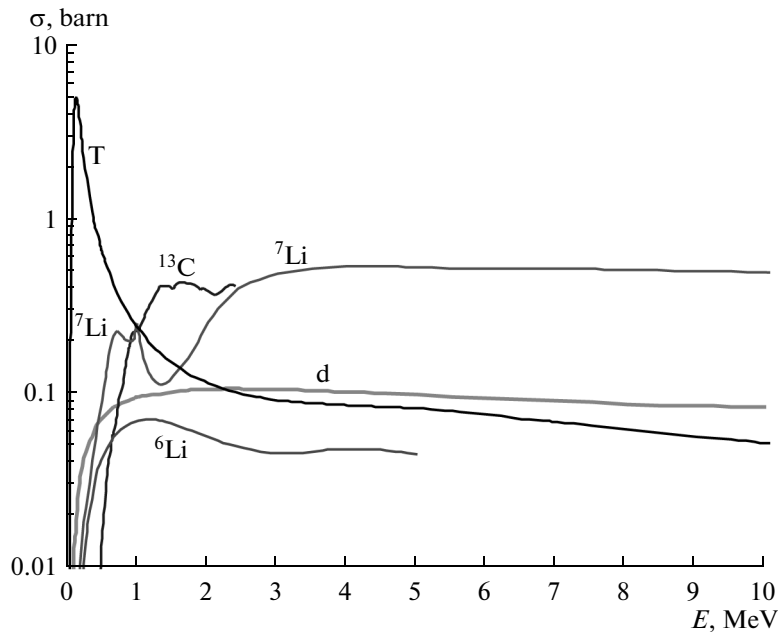


Fig. 3. The cross section of neutron generation in the interaction of deuteron beam with the target of deuterium, tritium, lithium-6, lithium-7, and carbon-13.

remaining two the attractiveness of the reaction ${}^7\text{Li}(p,n){}^7\text{Be}$ is still recognized, but it has been noted that all the problems of lithium target were already solved. Reaction ${}^9\text{Be}(p,n){}^9\text{B}$ can be also used, but a higher energy of protons is required to reach the comparable flux, which inevitably causes an increase in the energy of neutrons. Figure 2 shows the cross sections of reactions ${}^7\text{Li}(p,n){}^7\text{Be}$ and ${}^9\text{Be}(p,n){}^9\text{B}$. We can see that the cross section of the former reaction is three and more times higher than for the latter reaction. Thus, the most effective method of creating the neutron flux for BNCT is the use of reaction ${}^7\text{Li}(p,n){}^7\text{Be}$.

CHARGED PARTICLE ACCELERATORS FOR BNCT

First discussions and suggestions for creating accelerator BNCT sources were carried out at the end of the 1980s to the early 1990s [33–38]. We will discuss some of them. At the Massachusetts Institute of Technology (Boston, USA), Van de Graaff tandem accelerator LABA was built with stripping foil [39], and a 1 mA proton beam with an energy of 1.5 MeV was produced [40]. The disadvantage of the LABA accelerator is a short lifetime of the stripping foil (a few mA-h) and relatively low proton energy. The project of linear

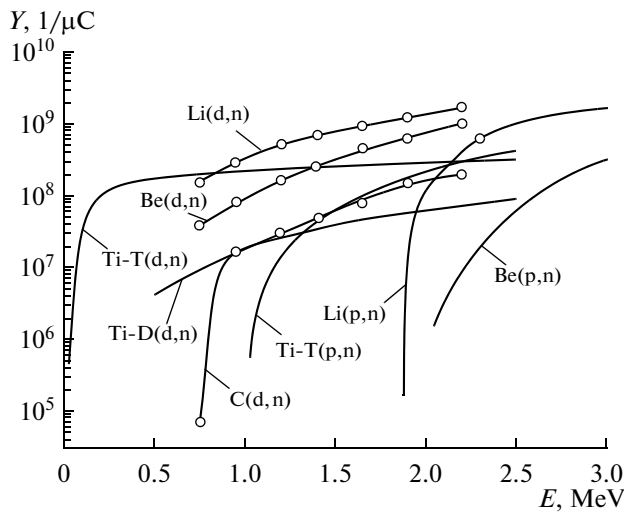


Fig. 4. Dependence of the neutron yield on the ion energy for several reactions.

accelerator with electrostatic quadrupoles has been proposed but not implemented at the Berkeley laboratory (US) [41, 42]. The proposed accelerator is large in size: it has a diameter of the accelerating tank of 2.4 m, and a length of 6.1 m. A proton quadrupole linacs [43–45] and a 2.5 MeV 1 mA tandem accelerator HVEE (High Voltage Engineering Europa) were also

proposed but not implemented. For research on BNCT at the University of Birmingham (England), a proton beam with an energy of 2.8 MeV and a current of 1 mA was obtained using Dinamitron [46]. At the moment, the team of British researchers has plans to upgrade the accelerator to increase the current up to 3 mA in order to initiate clinical trials of BNCT technique. Also, the efforts were made to use the Cockcroft-Walton KG-2.5 continuous-beam accelerator at the Institute of Physics and Power Engineering in Obninsk. An accelerator designed for obtaining 2.4 MeV 2 mA proton beam was constructed and manufactured at the Efremov Research Institute (St. Petersburg) in 1970 [47]. For many years it has been used for physical experiments.

Among the projects of the first decade of the 21st century, the following should be noted. An electrostatic quadrupole tandem accelerator to obtain a 2.5 MeV proton beam with a current of 20–30 mA [48, 49] is being developed at the Institute of Science and Technology, San Martin (Argentina). The success of the project is rather probable, but the accelerator will be more suitable for research purposes than for the introduction of BNCT into clinical practice. A giant project is being developed in Legnaro (Italy) to obtain exotic radioactive ion beams by irradiation of ^{238}U with fast neutrons obtained by damping the 100 MeV 1 mA proton beam onto the beryllium target. To use a

Table 1. Basic parameters of the neutron generation reactions

Reaction	Threshold energy, MeV	Particle energy, MeV	Yield, n/mA s	Neutron energy, keV	
				max	min
$^7\text{Li}(p,n)^7\text{Be}$	1.880	1.880	0	30	30
		1.890	6.3×10^9	67	0.2
		2.500	9.3×10^{11}	787	60
		2.800	1.4×10^{12}	1100	395
$^9\text{Be}(p,n)^9\text{B}$	2.057	2.057	0	20	20
		2.500	3.9×10^{10}	573	193
		4.000	1×10^{12}	2120	
$^9\text{Be}(d,n)^{10}\text{B}$	0	0	0	3962	3962
		1.500	3.3×10^{11}	4279	3874
$^{13}\text{C}(d,n)^{14}\text{N}$	0	0	0	4974	4974
		1.500	1.9×10^{11}	6772	5616
$^{12}\text{C}(d,n)^{13}\text{N}$	0.327	0.327	0	4	4
		1.500	6×10^{10}	1188	707
$d(d,n)^3\text{He}$	0	0	0	2451	2451
		0.120	3×10^8	2898	2123
		0.200	1.1×10^9	3054	2047
$t(d,n)^4\text{He}$	0	0	0	14050	14050
		0.150	4.5×10^{10}	14961	13305

5 MeV 30 mA proton beam in various applications, including BNCT, a beam deflection system is foreseen in the accelerating section [50]. The beryllium target is used for generating fast neutrons [51]. In the summer of 2014, a protocol of intent was signed providing for the establishment of the BNCT center in Pavia (Italy), equipped with a 2.5 MeV 20 mA proton accelerator manufactured by GT Advanced Technologies (Denver, Canada) [52]. On June, 10 2014, however, the company declared bankruptcy.

Significant efforts to implement BNCT into clinical practice have been undertaken in Japan. The first major step was taken by Ichigaya TRS (Japan), which in March 2005 signed a contract for 2 years with the Ion Beam Application company (Belgium) for the manufacture and commissioning of the world's first accelerator source of epithermal neutrons. Under the contract, the center had to be put into operation in Osaka in 2007. The company IBA, known as a global manufacturer of cyclotrons for producing short-lived isotopes for positron emission tomography, proposed the use of Dinamitron as an accelerator, which allows one to produce a proton beam with an energy of 2.8 MeV and a current of 20 mA. The execution of the contract was halted by mutual consent of the parties due to difficulties constructing the accelerator there. But despite termination of the contract, the studies at Dinamitron were continued [53] and in 2013 an agreement was reached on the delivery of the accelerator with a current of 15 mA at the University of Nagoya (Japan) [54].

The second project in Japan, funded from May 2005 to March 2008, was ERIT: a circular storage ring with a proton energy of 10 MeV and a current of 70 mA, with internal beryllium target [55, 56]. Although the completion of construction of the facility at the University of Kyoto (Japan) [57] was announced, at present there is no information on the continuation of the BNCT program. Perhaps this is due to the realization that one cannot get a neutron beam that meets the requirements of BNCT, particularly in the density of the flux.

The third project in Japan for Research Reactor Institute of Kyoto University (KURRI) was started in July 2007. A HM-30 cyclotron [58] with the beam shaping assembly has been designed, manufactured, installed, and commissioned in KURRI by the Company Sumitomo Heavy Industries, Ltd. A proton beam with a designed current of 1.1 mA and an energy of 30 MeV was obtained at the cyclotron weighing 60 t. As a result of the beam dump onto the beryllium target, the neutrons with energies up to 28 MeV are emitted. Further on, they are slowed down by the beam forming system creating epithermal neutron flux with an intensity of $1.2 \times 10^9 \text{ cm}^{-2} \text{ s}^{-1}$, which is two times higher than with previously operating reactor at the University of Kyoto, where 275 tests of BNCT were carried out [59]. Despite reaching the design param-

eters, the therapy was not carried out at the facility, since the generated neutron flux does not satisfy the BNCT requirements. This may be due to the presence of significant component of fast neutrons.

Currently, the University of Tsukuba in partnership with Mitsubishi Heavy Industry Co. and scientific organization KEK is constructing an 8 MeV 5 mA linac with the beryllium target [60]. This is done in the Japanese city of Tokai at the place where clinical trials of BNCT at the JRR-4 JAEA reactor were conducted previously.

A potentially attractive project is being developed by the Cancer Intelligence Care Systems for the National Cancer Center in Tokyo [61]. In January 2013, the company AccSys Technology, Inc. (California, USA—subsidiary of Hitachi) signed an agreement for the manufacture of a 20 mA 2.5 MeV linac. Use of the target with thin layer of lithium on palladium substrate is planned for the neutron generation.

TANDEM ACCELERATOR WITH VACUUM INSULATION

In 1998, a project of accelerator neutron source for BNCT was proposed, having three main ideas (Fig. 5) [62]. The first one was aimed at manufacturing a new type of tandem accelerator with vacuum insulation of electrodes for obtaining a high current proton beam. The second idea concerns the choice of reaction of neutron generation. Despite a low melting point, low thermal conductivity, and high reactivity of lithium, the ${}^7\text{Li}(p,n){}^7\text{Be}$ reaction should be used, since it is most efficient to produce epithermal neutrons. The third idea was in trying to apply a near-threshold neutron generation mode for therapy. In this case, because of the kinematic collimation, the generated neutrons are emitted predominantly forward and have a relatively low energy of about 40 keV. Figure 6 shows a photo of the tandem accelerator with vacuum insulation, while its schematic diagram is shown in Fig. 6 [63, 64]. To generate the beam of negative hydrogen ions with a current up to 5 mA and energy up to 23 keV, a source *I* developed by Y. Belchenko [65, 66] is used. This is a surface-plasma source using the Penning discharge with hollow cathodes. The negative hydrogen ion beam coming from the source is bent through an angle of 15° in a magnetic field. Further on, the beam is focused by a pair of magnetic focusing lenses, injected into accelerator and accelerated up to 1 MeV. In stripping gaseous target 7 mounted inside high-voltage electrode 2, negative ions of hydrogen are converted into protons, which are then accelerated by a potential of 1 MV (the same potential) to an energy of 2 MeV and transported towards the neutron-generating target. Two pairs of quadrupole lenses with the magnetic field gradient up to 400 Gs/cm are mounted in the high energy beam transporting channel with a field length of 20 cm, and a bending magnet (90°) with a bending radius of 45 cm, an intensity of the magnetic

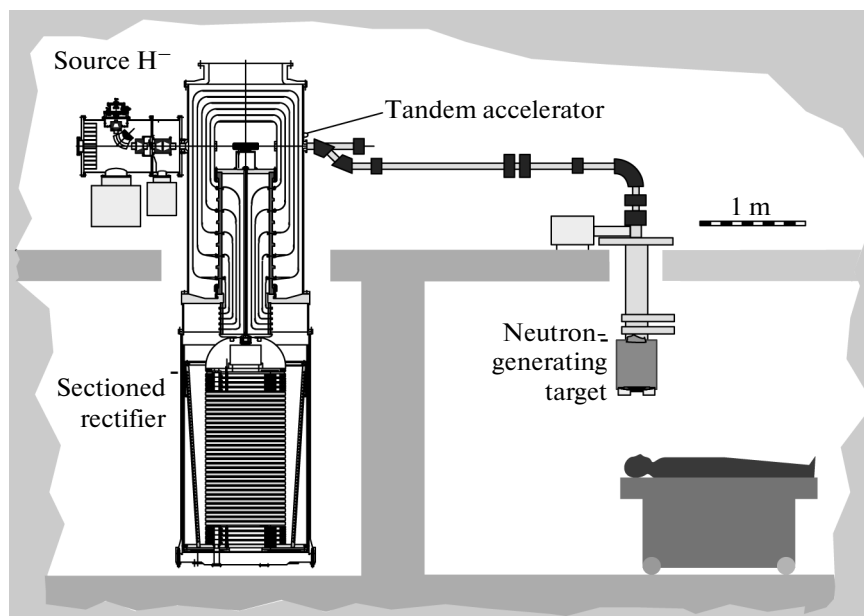


Fig. 5. Schematic diagram of the neutron source based on tandem accelerator with vacuum insulation.



Fig. 6. Photo of a tandem accelerator with vacuum insulation.

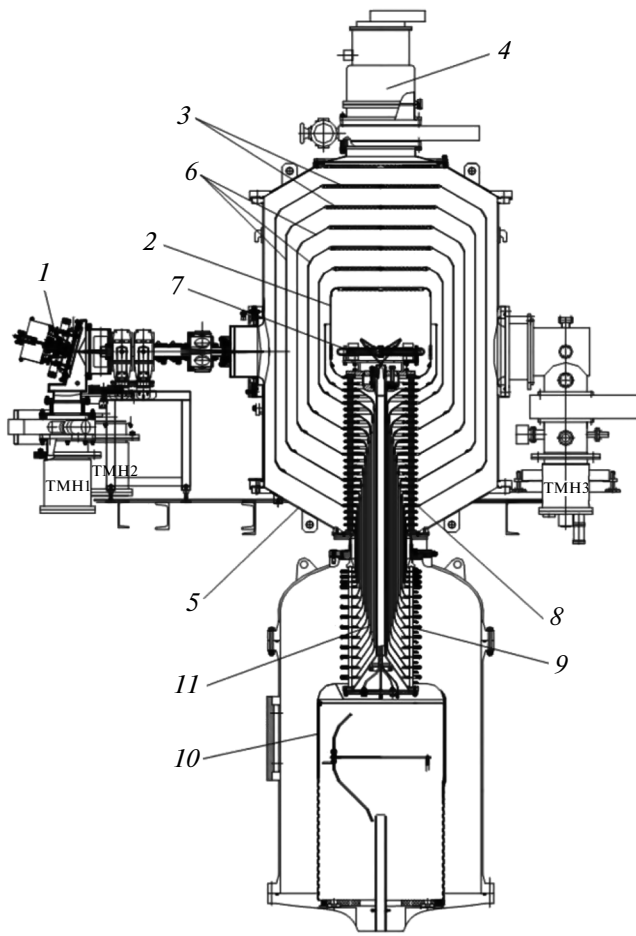


Fig. 7. Tandem accelerator with vacuum insulation: 1—source of negative hydrogen ions; 2—high-voltage electrode; 3—blinds of electrode-screens; 4—cryogenic pump; 5—vacuum tank; 6—intermediate electrode-screens; 7—rechargeable gas target; 8—vacuum part of bushing; 9—gaseous part of bushing; 10—high-voltage power supply; 11—inner coaxial cylinders, connecting the equipotential electrodes of the gas and vacuum parts of the insulator.

field ~ 3 kG, and a decline index of 0.5. The magnetic scanning system performs the beam scanning over the target by using a uniform magnetic field with a strength of 500 Gs at a length of ~ 20 cm, rotating at a frequency of 100–2000 Hz [67] (not shown). The voltage is fed from high-voltage power supply 10 (the larger part is not shown) on high-voltage electrode 2 and five intermediate electrodes of accelerator 6 through bushing 8 and 9, in which the ohmic divider is mounted. As the source of high-voltage power supply, a rectifier of an ELV industrial electron accelerator (developed, and manufactured at BINP)—which is being widely used in process applications in many industrial enterprises and companies in Russia and abroad—is used [68]. Gas pumping is carried out by a turbo pump mounted near the ion source and at the exit of accelerator, and using cryogenic pump 4

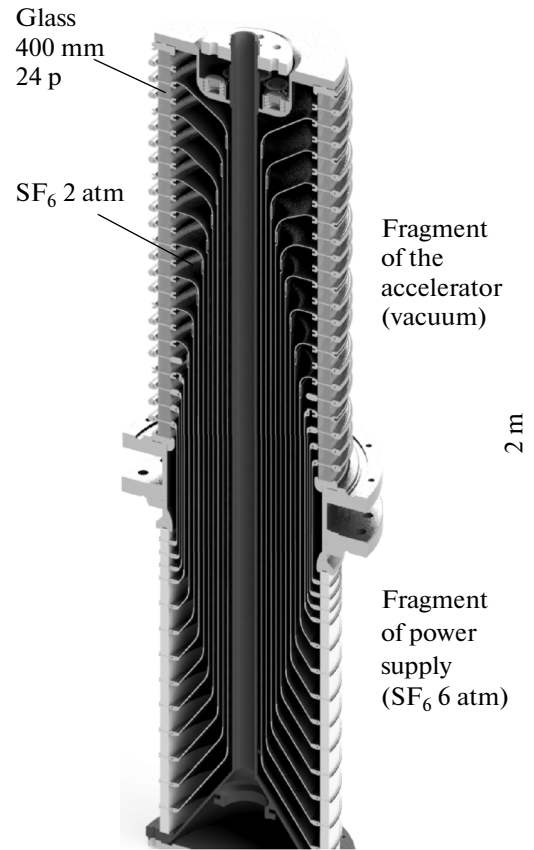


Fig. 8. Bushing.

through the blinds of electrodes 3. Diameters of the vacuum tank and the high voltage electrode of accelerator are 1400 and 600 mm, respectively.

A vacuum part of bushing (Fig. 8), made of 24 glass-ring vacuum-tightly-contracted isolators with a diameter of 400 mm and a height of 35 mm, is made by using intermediate electrodes and sealing made of indium (rubber sealing from 2012). The gaseous part of the isolator, located in the tank of high voltage rectifier, is composed of 14 ceramic rings with a diameter of 400 mm and a height up to 60 mm, glued to their electrodes. The tube which compacts two parts into a single bushing with a force of 5 tons is located on the axis. The inner part of bushing is filled with sulfur hexafluoride (SF_6) at a pressure up to 0.3 MPa; the pressure in high-voltage rectifier tank is up to 0.8 MPa. Resistive divider located around the gaseous side of the bushing distributes the high voltage potential over the intermediate accelerating electrodes through the electrodes of gaseous isolator, metal thin-walled pipes coaxially arranged inside the isolator, and electrodes of the vacuum isolator. The potential is distributed on the electrodes of vacuum isolator which are not connected electrically with coaxial tubes by using the resistors located inside the vacuum section of bushing.

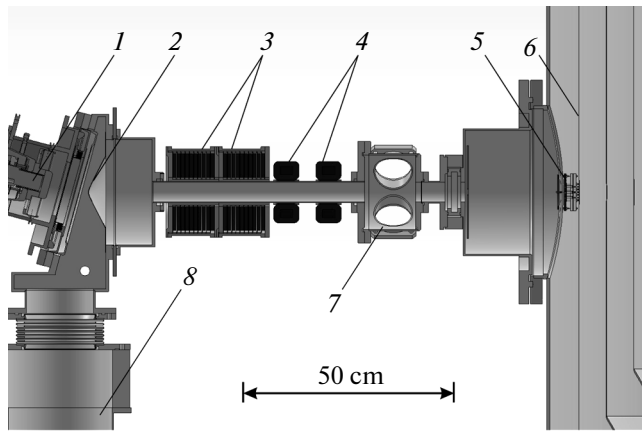


Fig. 9. Schematic layout of the experiment: 1—source of negative hydrogen ions; 2—cone diaphragm; 3—focusing magnetic lenses; 4—corrector; 5—beam detector; 6—the first electrode of the accelerator; 7—diagnostic chamber; 8—TMN pump.

In this tandem accelerator with vacuum insulation, the accelerating tubes as such are absent. The insulator is removed from the beam path of acceleration for a considerable distance, that, along with the implementation of gas pumping through the blinds of the electrodes outside the accelerating gap, gives us a hope for obtaining a high-current proton beam. The accelerator has a high rate of acceleration of charged particles, but there are two specific problems.

The first problem stems from the fact that high energy is stored in the accelerating gaps due to the large area of electrodes. High-voltage strength of the centimeter vacuum gaps was further investigated, since it was known that the breakdowns with released energy of more than 10 J lead to a drop in the strength of the high-vacuum millimeter gap [69]. It was found that the breakdowns with stored energy up to 50 J do not reduce the high strength of 45 mm gap, and until the electric field strength reaches a value of 60 kV/cm, the dark current value is acceptably small [70]. These results together with the results of the examination of the dynamics of high-voltage breakdown elements [71] served as the basis of design of the accelerator with an energy stored in the gap up to 30 J and a field strength of 25 kV/cm. As a result of the training of all gaps using a specially made device, the required voltage of the accelerator (1 MV) was obtained [72]. The behavior of the dark current was studied and its reduction to an acceptable level by means of long exposure under the voltage was carried out [73]. Detailed results of the study of the high-voltage strength of tandem accelerator with vacuum insulation are presented in the thesis by Sorokin [74].

The second specific issue is the rapid rate of acceleration of ions, due to which the input electrostatic lens of accelerator is too strong. It was necessary to refocus the injected beam of negative hydrogen ions

with an energy of around 21 keV before the accelerator entrance lens in order to accelerate it with a rate of 25 keV/cm in the narrow accelerating channel. In the design of the ion-optical path, different methods of injection of the ion beam into accelerator were discussed, and it was decided to use the magnetic lenses [75]. To study the injection, a multichannel detector of the beam was made and installed in front of the inlet of the first accelerating electrode of accelerator (Fig. 9). Measurements of the beam current profile depending on the current of magnetic lenses were carried out, which allowed us to determine the transverse ion temperature at the plasma boundary source: about 1 eV. It was found that total compensation of spatial charge is implemented in the transporting channel [76, 77]. The result is the implementation of the injection of the beam of negative hydrogen ions into accelerator and its acceleration without significant losses.

In the design of the accelerator, different types of stripping targets were considered and the gas target has been chosen [78]. It is made in the form of cooled cylindrical copper tube of 400 mm length with an inner diameter of 16 mm with the inflow of the argon in the middle and installed inside the high voltage electrode on the bushing. The gas supply into the target is performed using a five-liter bottle placed in the electrode of high voltage power supply through the buffer volume in which the gas flow rate is controlled by opening an electromechanical valve. The gas enters into the stripping target from the buffer volume through precision needle valve and a tube with a length of 2 m and an inner diameter of 4 mm located inside the bushing. The characteristic time of gas outflow is 500 s. Stripping of the negative hydrogen ions into the protons is studied experimentally by measuring the beam current at the exit of the accelerator when changing gas injection rate into the target. A good agreement between the experimental and calculated data was found [79, 80]. A method of calibrating the stripping gas target is proposed and implemented, based on the measurement of gas inflow at which the proton current is equal to the current of non-recharged negative hydrogen ions at the exit of the accelerator.

These investigations enabled us to significantly increase the proton beam current. In the initial experiments, the characteristic value of current was 100–200 μA [81, 82]. Currently, the proton beam with a current up to 1.6 ± 0.007 mA in the long-stable mode (over 1 h) is obtained (Fig. 10) [83]. The beam is characterized by the high stability and high energetic monochromaticity of current: 0.1%. The monochromaticity was measured by two methods. In the first method, the generation of 9.17 MeV γ -quanta from the reaction $^{13}\text{C}(p,\gamma)^{14}\text{N}$ is performed when dumping the proton beam with an energy of 1.747 MeV onto a graphite target enriched in the isotope of carbon-13. The rate of γ -quanta counting depending on the proton beam energy was measured by using a BGO

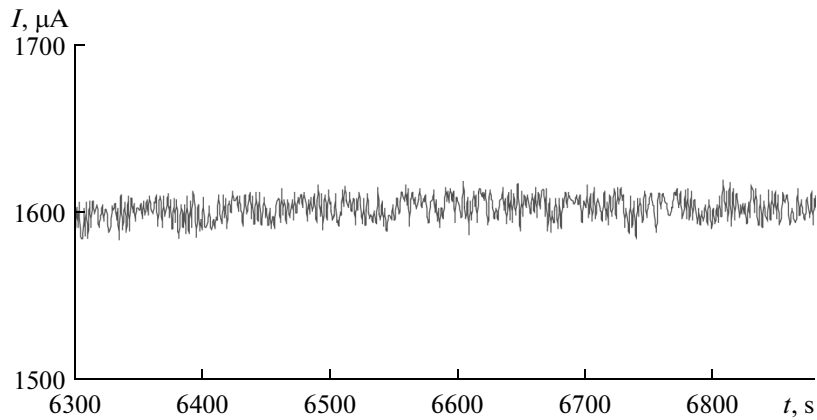


Fig. 10. Time dependence of the proton beam current.

γ -spectrometer. Since the resonance of γ -quanta production is very narrow (± 0.9 keV [84]), the slope of the excitation curve is entirely determined by the instability of proton energy. According to this curve, the energy spread of protons is ± 2 keV. In the second method, the long-term stability of the proton beam energy was assessed by measuring the neutron spectrum with the help of time-of-flight technique: its value turned out to be better than ± 5 keV [85]. The proton beam energy is measured using the resistive voltage divider of high voltage power supply. For divider calibration, the threshold reactions $^{13}\text{C}(p,\gamma)^{14}\text{N}$ and $^7\text{Li}(p,n)^7\text{Be}$ are used. The accelerator enables researchers to obtain a proton beam with an energy from 600 keV to 2 MeV.

To conduct the therapy, the proton beam current should be of at least 3 mA. The attempts to increase the proton beam current due to injection of the beam of negative hydrogen ions with a current of 2 mA or due to higher gas inflow rate onto the stripping target led to frequent breakdowns of the accelerator by the full voltage, making it impossible to obtain stable proton beam. An increase in the current through the accelerating gap was found with increasing gas inflow onto the stripping target and a growth in the absorbed dose rate of bremsstrahlung (Fig. 11) [86]. It turns out that gas delivery to the stripping target during injection of a 1.55 mA beam of negative hydrogen ions leads to an increase in the current in the accelerating gap by $500 \mu\text{A}$ with unhooked cryogenic pump (and by $250 \mu\text{A}$ with enabled cryogenic pump) and an increase in the dose rate of bremsstrahlung by three times.

Using a special detector fabricated in the form of two concentric annular discs and mounted at the accelerator entrance by the side of high voltage electrode, a flow of positive ions towards the injected ion beam was registered at the periphery, and its growth with increasing gas inflow to the stripping target. As a result, it was established that the ionization of residual

and stripping gas by the ion beam (mainly) at the accelerator entrance and penetration of the portion of positive argon ions emitted from the stripping target into the accelerating gap of the channel lead to the appearance of a current accompanying the beam of

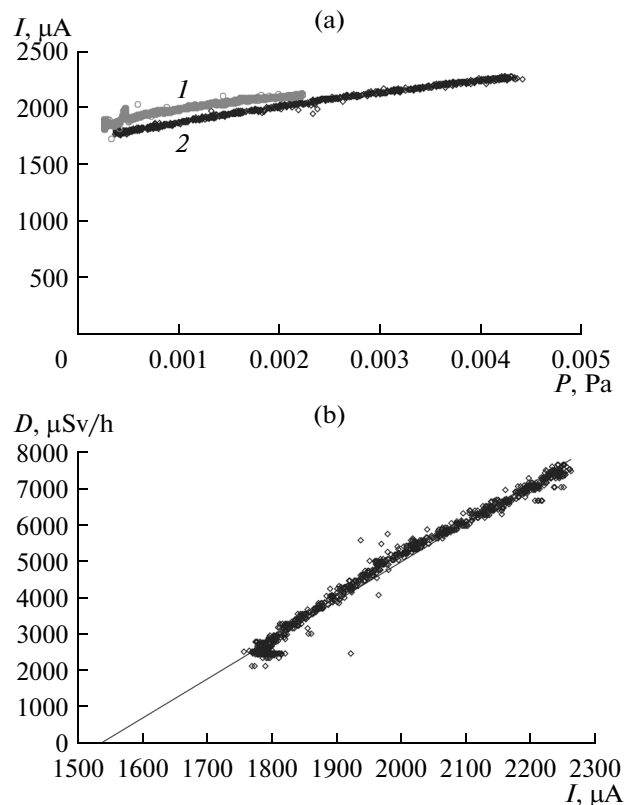


Fig. 11. The accelerating gap current as a function of the residual gas pressure with an increase of the gas inflow onto the stripping target: (1) with cryogenic pump on, (2) with cryogenic pump off (a); (b) the absorbed dose of bremsstrahlung radiation as a function of the current in the accelerating gap.

ions [86]. This current contributes to the breakdowns of accelerator caused by the total voltage. When the cryogenic pump is turned off, it is possible to provide a 50% stripping of the beam without breakdowns. When the cryogenic pump is turned on, the magnitude of an accompanying current reduces by approximately two times and allows one to obtain 90% stripping of the beam. A further increase in the current of the proton beam is possible while improving the vacuum conditions in the accelerating gap by the planned installation of an additional cryogenic pump at the entrance flange of the accelerator and modification of the stripping target. Modification of the target aims at reducing the gas flow, ultraviolet radiation, and the flow of positive argon ions into the accelerating gap. Modification of the target assumes that it shifts upwards or tilts relative to the beam line using permanent magnets arranged in the space between the diaphragms of the high voltage electrode and the ends of the tube with stripping target, as well as the implementation of differential pumping by the installation of turbo pump inside the high-voltage electrode [87].

NEUTRON-GENERATING TARGET

Different types of lithium neutron-generating targets were examined: jet-like, ribbon-like, spherical, volume, rotating, and stationary [88–92]. In accordance with the requirements of high neutron flux and spectral characteristics, the necessity of patient positioning near the neutron production region and the usage of a minimum amount of structural material in the target unit become important. When selecting the final design of the target for practical implementation, it was taken into account not only its complexity, but also an opportunity of forming therapeutic neutron beam with the best quality. As a result, a stationary target was chosen for the practical implementation, despite its complexity in manufacturing, but having an optimal quality.

Lithium has a low melting point (182°C), low thermal conductivity (71 W/m K in the solid state and 43 W/m K in the liquid state at the melting point), and high chemical activity. Neutron generation in the reaction ${}^7\text{Li}(p,n){}^7\text{Be}$ is accompanied by the formation of radioactive ${}^7\text{Be}$ isotope. The interaction of a proton beam with lithium leads to the generation of 0.478 MeV gamma quanta resulting from the inelastic scattering of protons on the nuclei of lithium, γ -quanta with energies of 16–19 MeV during the radiative decay of the ${}^8\text{Be}$ nucleus in reaction ${}^7\text{Li}(p,\gamma){}^8\text{Be}$, and α -particles as a result of thermonuclear reactions ${}^7\text{Li}(p,\alpha)\alpha$ and ${}^6\text{Li}(p,\alpha){}^3\text{He}$ with an energy yield of 17.347 and 4.021 MeV.

An optimal stationary target should have the following properties [93].

(1) Neutron-generating lithium layer should be thin enough for the protons slowed down to the

threshold of neutron generation. This will significantly reduce the associated flow of 0.478 MeV γ -quanta and reduce the surface temperature of lithium.

(2) Neutron-generating lithium layer should be made of pure lithium for maximum neutron yield. The neutron yield from hydride, oxide, and lithium fluoride is less than that of pure lithium by 1.43, 2, and 3.3 times respectively.

(3) Neutron-generating lithium layer should be in a solid state to prevent the spread of lithium vapor and radioactive isotope beryllium-7 inside the setup.

(4) The substrate onto which the lithium neutron-generating layer is deposited should be thin. This will allow researchers to put the optimum moderator close to the place of neutron production and create a therapeutic neutron beam of better quality.

(5) The substrate must be cooled intensively to maintain the layer of lithium in the solid state when it is heated by a powerful proton beam.

(6) The substrate must be resistant to radiation damage.

(7) The substrate should be simple to manufacture.

(8) The substrate should be easily removable for its utilization after activation.

To construct an optimal target, it was necessary to solve the following problems: (i) deposition of a thin layer of pure lithium of controlled thickness, (ii) ensuring effective heat removal to preserve the lithium in the solid state when heated by a powerful proton beam, (iii) finding the substrate materials to be most resistant to radiation damage, (iv) developing the target design with the possibility of easy removal of the substrate of the target with an activated lithium layer, and (v) disposal of activated part of the target.

ENSURING EFFECTIVE HEAT REMOVAL

At first, it was planned to manufacture the target with a diameter of 5 cm and a power of 25 kW of a proton beam. In this case, the only possibility to maintain the target temperature below the lithium melting point was cooling by liquid metal. Gallium and mercury provide about the same heat removal, but gallium was chosen for cooling since it requires a smaller pumping pressure [62]. The first variant of the target is a molybdenum foil of 0.2 mm thickness, and of 64 mm diameter, bonded to the ribs of the disk of ARMCO steel by diffusion welding, in which the channels for coolant flow have been made [94]. The hydraulic tests conducted have shown the reliability of welding to the edges of the foil up to a water pressure of 4 atm. Liquid metal cooling system has been developed, produced, and tested, including the pump for pumping liquid gallium, liquid metal circuit with switching devices, the heat exchanger, speedometer of the metal velocity, and indicator of pressure distribution. Magnetic clutch was manufactured, which provides non-contact torque transmission to mechanical pump that has

been evacuated and filled with liquid metal volume of the liquid metal circuit. Thermal testing of the target cooled by water or liquid gallium was conducted on an ELV electron accelerator at an electron energy of 1.4 MeV and a power up to 20 kW [68]. Using water cooling, the heat removal rate reached up to 650 W cm^{-2} . The cooling using liquid metal enabled researchers to maintain a lower temperature of the target surface, compared with water-cooled one [88]. But during the tests, the destruction of target occurred, and through the holes formed in the foil and steel disc a portion of gallium flowed out. To clarify the reasons of the target destruction, a molybdenum foil was separated from the beam receiver made of steel. A significant corrosion of the ARMKO steel was found, but the molybdenum foil corrosion was not observed. A possible reason of the damage of the target was the leakage of some amount of gallium through the notch for thermocouple as a result of corrosion of a steel wall. Therefore, the use of liquid metal cooling led to the destruction of the target due to the lack of chemical resistance to gallium of the ARMKO steel when heated.

Further prospect to ensure effective cooling was either in experimental finding of the materials resistant to gallium for a long time, or in solving the problem of cooling with the use of water. The paradigm of using the target with a diameter of 5 cm was reconsidered. Kononov performed calculations similar to those presented in [95], at proton energies of 1.91 MeV and different diameters of the target [96]. It was found that an increase in the target diameter effectively suppresses the dose of recoil protons on the surface of phantom at an insignificant decrease in the therapeutic dose inside it, caused by reaction $^{10}\text{B}(n,\alpha)^7\text{Li}$. Thus, an increase in the diameter from 5 to 10 cm decreases the dose of recoil protons on the surface of phantom by 25%, while the therapeutic dose reduces by 12%. Thus, increasing the diameter of the target causes a certain decrease in the dose rate, and enables researchers to apply water as a coolant to maintain the lithium layer in the solid state.

Thermal testing of the target made of a copper disc with a thickness of 5 mm with rectangular cooling channels with dimensions $3 \times 2 \text{ mm}$, held tightly to a titanium housing, was conducted by using the Ohmic heater with a power up to 20 kW. Ohmic heaters were made of niobium or tantalum plate with a thickness of 0.1 mm, in which the strips of 2 mm width in the form of an Archimedean spiral were cut (with a gap of 0.2 mm) using the electric spark method (Fig. 12). Then, using an electrochemical microarc method, the heater was covered with a thin layer of metal pentoxide (Nb_2O_5 and Ta_2O_5 ; 5–10 μm), providing an insulation voltage of no less than 300 V. The heater resistance is of the order of 1 Ohm. A current lead is provided using the molybdenum rods pursued by springs. The heater is powered by a stabilized source with a current up to 100 A. The heater is tightly pressed to the target



Fig. 12. Ohmic heater.

through a BeO isolator 1 mm thick with small heat conductivity, hampering the cooling in other side. It should be noted that the use of stabilized power supply is necessary, except when there is significant component of the AC, since the displacements of the heater lead to the abrasion of isolator and the breakdown of the heater. The target is cooled during the flow of distilled water in the channels at a speed of 5 m/s. The temperature of the target surface was measured with a thermocouple sandwiched between the insulator and the target in the disc recess.

Figure 13 shows the results of the experiment. One can see three regimes of heat removal on experimental curve: (i) up to 250 W/cm^2 —turbulent water flow without boiling, in good agreement with calculation; (ii) from 250 to 400 W/cm^2 —turbulent water flow with bubble boiling, when the temperature is nearly constant; (iii) 450 W/cm^2 —turbulent water flow with film boiling when the cooling is disrupted and the temperature quickly rises. When the density of heating power reaches 318 W/cm^2 , the target surface is heated up to 200°C at a water velocity of 3 m/s. This temperature is somewhat less than the calculated temperature, since the mode of nucleate boiling was already implemented: this is detected not only by the plateau on the graph, but also due to the characteristic sound at the time of experiment. Of course, the heat removal with nucleate boiling is more efficient; however, to obtain a lower temperature and for safety reasons, the turbulent flow of cooling water without boiling should be taken as the working mode of cooling. An accidental local overheating can lead to nucleate boiling, but this will not lead to a significant increase in the temperature. A rather extended plateau on the graph corresponding to the nucleate boiling provides almost double the power supply to the heating power, at which

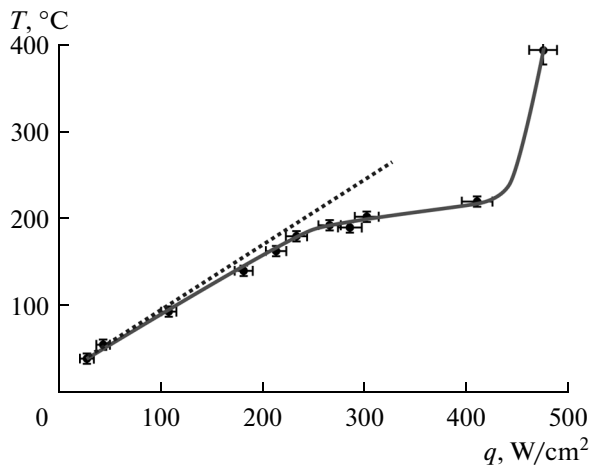


Fig. 13. The surface temperature T of the target as a function of the power density of heating q at a cooling water velocity of 3 m/s: solid line—experiment, dashed line—calculated curve for the turbulent flow without boiling.

the failure of heat removal is possible. The thermal tests and calculations conducted make it possible to conclude with confidence that, during absorption of 25 kW proton beam in the target with a diameter of 10 cm, the lithium layer can be maintained in the solid state when cooling the target by turbulent water flow at a speed of about 10 m/s [97].

RADIATIVE BLISTERING

Since the lithium layer in the neutron-generating target is thin, the protons are not absorbed in it. They are only slowed down to an energy slightly lower than 1.882 MeV. Further slowdown and absorption of the protons occur in the substrate material on which a lithium layer is deposited. Major energy losses of protons are caused by the process of ionization of the atoms of substance, the cross section of which decreases with decreasing energy. Due to this, the proton loses the major part of its energy before the moment of stopping (Bragg's peak). Stopping of protons with energies of the order of 2 MeV has a nearly linear dependence: their total and projected ranges differ by no more than a few percent. Thus, the proton ranges with an energy of 2 MeV in Li equals 160 μm , 50 μm in Be, 44 μm in Al, 30 μm in Ti, 23 μm in V, and less than 20 μm in Fe, Cu, Mo, W [98]. In handbook [98], along with the graphs of the range-energy dependence, the graphs of the projected ranges are also presented. Both graphs merge, starting from the energies of several hundreds keV for materials of light elements (Li, Be, C, Al, etc.) and from the energies of order 1–2 MeV for materials of heavy elements (Ta, W, Au, etc.).

The method of calculation of the longitudinal distribution of high-energy ions in the matter was proposed and described in [99]. In this work as an example, the longitudinal stopping distribution of 1 MeV

protons in ^{28}Si is presented, which shows that the width of this distribution at a half height of the maximum does not exceed 10%. Thus, in the case of monoenergetic beam, the protons are all practically absorbed at the same depth, forming the region of an increased concentration of hydrogen.

It is known [100, 101] that at the target irradiation fluences of 10^{14} – 10^{17} ion/cm² the agglomeration of trapped gas atoms occurs, leading to the formation of gas bubbles and volumetric expansion of the material (up to 10–15%). With further irradiation (10^{17} – 10^{20} ion cm^{−2}), the saturation of implanted gas trapped in the solid body occurs, the surface layer can be deformed up to the formation of blisters (plate-like domed swellings of the surface layer), and exfoliation of flakes occurs due to increasing the internal gas pressure and the lateral compressive stress. The appearance of developed surface of the target can not only lead to an increased evaporation of lithium because of reduced thermal conductivity, but also makes the target unfit. In [100, 101], the critical dose of hydrogen blistering (10^{18} – 10^{19} ions/cm²) is reported, and the authors stress that the hydrogen blistering is observed mainly for metals which poorly dissolve hydrogen (Al, Mo, Fe, Cu, Ag, W, Pt, Au). In metals which dissolve hydrogen well (alkaline, alkaline-earth, Ti, Ta, Nb, V, Ni, Pd), the hydrogen blistering is typically not observed. At a current of 10 mA and 10 cm target diameter, the fluence rate equals 8×10^{14} cm^{−2} s^{−1}. The lower boundary of the hydrogen blistering (10^{18} cm^{−2}) is reached in about 20 minutes, which is less than the scheduled time of exposure, so the blistering can significantly limit the use of some materials as the targets. Since the experimental data on hydrogen blistering are extremely poor, and radiation damage of the target depends on many factors (type and energy of ions, the material and target temperature, gas solubility, crystallographic orientation of the target) and can manifest itself in different ways (with the formation of blisters, flaking, swelling), further studies were necessary for selecting the optimum material of the beam absorber. In what follows we use the terminology [100], when the term “blistering” means not only the bubble formation, but also the processes of flaking and swelling. In addition to this, a radiative bubble formation is also called “blistering,” but we do not consider the formation of bubbles on the surface of material which appear upon material processing in gaseous medium.

First, we note that the relationship between the critical blistering dose and the ion energy E is given in [100]. The dependence rises as $E^{0.4}$. Also in this work the plot of the critical dose of blistering as a function of the target temperature is given, showing the differences on the order of magnitude.

In addition to the ion energy and the target temperature, the diffusion of hydrogen in material determines the critical dose for target operation. The characteristic diffusion coefficients of hydrogen atoms in metals

Table 2. Diffusion coefficients of hydrogen atoms in metals

$T, ^\circ\text{C}$	$D, 10^{-6} \text{ cm}^2 \text{ s}$						References
	$\alpha\text{-Fe}$	Ta	Cu	V	Al	Pd	
20	1	0.8	0.002	4	0.0002	3	[102]
100			0.039				[103]
200		10		1	1	20	[102]

Table 3. Fluence of the blister formation in metals during proton beam irradiation

Material	Fluence of blister formation, 10^{18} cm^{-2} (the water temperature ($^\circ\text{C}$) on the outlet is given in the parenthesis)	
	at an energy of 100 keV	at an energy of 200 keV
Cu	0.4 (24)	1.42 (22)
	0.9 (95)	10 (95)
W	2–4 (95)	
Pd	8.5 (95)	
Ta	>230 (20)*	>58 (28)*
V	>120 (22)*	>
$\alpha\text{-Fe}$	240 (94)	205 (29)
		210 (93)

* Blistering is not observed up to the fluence registered in the experiment.

are shown in Table 2. It can be seen that the diffusion of hydrogen in such metals as Fe, Ta, V, and Pd, is significant, and we may hope to obtain high values of fluence before blistering onset. In aluminum and copper, the diffusion of hydrogen is weaker and blistering is expected to be at a much less fluence. First, to study the development of the surface relief at the test-bench, the copper and tungsten beam receivers were irradiated by powerful pulsed proton beams up to fluences of 10^{17} , 10^{18} , and 10^{19} cm^{-2} [96]. The beam receiver was intensely cooled with water. The energy of the proton beam in these experiments was 50 keV. The trajectories of protons with an energy of 50 keV are not so rectilinear in the absorber compared to the protons with an energy of 2 MeV. Nevertheless, the appearance of the density maximum of the captured atoms is possible at a depth. Thus, the total range of 50 keV proton in copper equals $0.45 \mu\text{m}$, the projected range is $0.12 \mu\text{m}$, and the standard deviation of the distribution is $0.075 \mu\text{m}$ [98]. Some inadequacy of this experiment is related not with scattering, which leads to a wider distribution of particles, but with low penetration depth comparable with the roughness of material. Hence, the surface of the beam receiver has been processed with diamond tools to obtain a mirror-like surface. It was found that a fluence of 10^{17} cm^{-2} does not result in any visible changes on the surface of receiver. The impact of a fluence of 10^{19} cm^{-2} causes visible modifi-

cation of the surface: (i) the color of the tungsten receiver significantly changes while the copper receiver weakly changes the color; (ii) the copper surface irradiated by protons becomes dull and scatters light well, while the tungsten surface remains a mirror-like.

Next, the investigation of blistering during irradiation of different metals was carried out (Ta, V, Pd, Fe, Cu, and W) using a proton beam with an energy of 100 or 200 keV, a current of about 1 mA, and the density of current about 1 mA cm^{-2} . The results were published in [104] and they are shown in Table 3. One can see that copper and tungsten are the least radiation-resistant elements. Palladium, despite high diffusion coefficient for hydrogen, proved to be not resistant to blistering. The highest resistance to blistering is seen in α -iron, vanadium, and tantalum.

Similar experiments were also conducted at the Namur University (Belgium). The protons were accelerated up to an energy of 1.85 MeV, the most appropriate for this study. However, because of the low beam current ($4\text{--}7 \mu\text{A}$), the proton beam was focused on the target into a small spot with an area of 0.01 to 0.1 mm^2 in order to achieve the desired fluence in a reasonable time. It was found that on such materials as Cu, Al, and W, the bubbles arise at a fluence of $2 \times 10^{19} \text{ cm}^{-2}$. On palladium, blistering was not observed at a fluence of $6 \times 10^{19} \text{ cm}^{-2}$, but it was observed upon a fluence

Table 4. The critical fluence of blistering in copper

Parameter	References				
		[104]	[104]	[105]	
Energy, keV	50	100	200	325	1850
Dose, 10^{18} cm^{-2}	From 0.1 to 10	0.9	10	5.2	20
Dose at 2 MeV, 10^{18} cm^{-2}	From 0.4 to 40	3	25	10	20

of $2 \times 10^{20} \text{ cm}^{-2}$. On V, Fe, and Ta blistering was not observed at fluences 6×10^{19} , 10^{21} , and $1.6 \times 10^{21} \text{ cm}^{-2}$, respectively. In [105], it was claimed that blistering of the copper surface irradiated by protons with an energy of 325 keV occurs at fluences greater than $5.2 \times 10^{18} \text{ cm}^{-2}$. In [106], the authors pointed out that under irradiation by 1.76 MeV protons of tantalum layer with a thickness of 0.13 mm on copper substrate, blistering was not observed at a fluence of 10^{19} cm^{-2} .

We estimate the critical dose of blistering for different materials irradiated by protons with an energy of 2 MeV. Let's start with copper. Table 4 summarizes the critical dose of blistering at different proton energies. From the results obtained in BINP at energies of 100 and 200 keV, those were taken which correspond to a higher temperature of the target being closest to the planned operation mode of the target. The last line of the table shows the assessment of the critical dose of protons at an energy of 2 MeV, assuming the fluence dependence on the energy of the form $E^{0.4}$. Despite large variations in assessments of the critical dose of the hydrogen blistering in copper at a 2 MeV proton irradiation, the critical dose turns out to be an order of magnitude greater than the minimum value reported in [100]. With some degree of reliability we can assume that the critical dose of blistering in copper at 2 MeV proton irradiation has a value of $2 \times 10^{19} \text{ cm}^{-2}$. Analogously to that, one obtains that the critical dose of blistering under proton irradiation with an energy of 2 MeV in aluminum and tungsten has the same value as in copper, namely $2 \times 10^{19} \text{ cm}^{-2}$. In palladium this dose equals $6 \times 10^{19} \text{ cm}^{-2}$. In V, Fe, and Ta one can expect that blistering is absent up to a fluence of $5 \times 10^{20} \text{ cm}^{-2}$.

Table 5. Estimated radiation time resistance of the targets of various materials with respect to the blistering during proton irradiation with an energy of 2 MeV, current of 10 mA, target diameter of 10 cm and temperature of 150°C

The substrate material of the target	Time of blister appearance, h
Cu, Al, W	7
Pd	20
V, Ta, α -Fe	>200

In summary, Table 5 shows the irradiation time of a target with a diameter of 10 cm and a characteristic temperature near 150°C needed for production of blistering in the proton beam with an energy of 2 MeV and a current of 10 mA. One can see that for all materials the onset time of blistering is greater than the planned time of therapy (1 h). Therefore, from the viewpoint of blistering, one can use almost any material as the substrate material. However, under the conditions of oncological clinic, the substrates of copper have to be replaced after each patient or, at best, every day. The substrates of vanadium, tantalum, or pure α -iron can be replaced much less often: once a month or once every several months.

Thus, radiation blistering restricts operation time of the target substrate, but it is not critical. During the therapy one can use both a copper substrate, which is easy to manufacture and has a better conductivity for effective heat removal, and the substrates of V, Ta, or α -Fe, requiring much more frequent replacement. It is worth noting one more aspect, which is important in practical medicine. When using the substrates which are resistant to radiation blistering, a successive accumulation of the radioactive beryllium-7 isotope will take place. Each patient, except the first, will receive an additional dose of the radioactive beryllium-7 isotope, formed by irradiating previous patients. Though this dose is small, it is present. It can be avoided for each patient using a new copper substrate with freshly deposited layer of lithium.

GAMMA-RADIATION

The inelastic scattering of protons by nuclei of lithium is characterized by a cross section of 40–120 mb with resonances at energies of 1.05, 2.05, and 2.25 MeV, and results in significant γ -quanta flux with an energy of 0.478 MeV, comparable to the neutron flux [107]. Table 6 shows the dependence of γ -quanta yield on the proton energy for thick lithium target, in which the proton is completely stopped, and for thin target, in which the proton is moderated only up to 1.882 MeV—the threshold energy of the neutron generation. It can be seen that the use of thin target reduces an undesired γ -quanta flux.

When using thin lithium target the proton absorption should be carried out in the matter in which reactions (p,γ), ($p,p/\gamma$), ($p,n\gamma$), and ($p,\alpha\gamma$) do not lead to

an appreciable yield of γ -quanta [108]. To determine the structural material of the substrate of neutron-generating target with minimum yield of accompanying γ -radiation, an experimental study of radiation under absorption of 2 MeV protons was carried out in different materials. A specially manufactured vacuum volume was set instead of neutron-generating target, consisting of stainless steel pipes with an inner diameter of 100 mm and a wall thickness of 2 mm, the bottom of water-cooled copper disc of 16 mm thick, and a quartz glass tube for monitoring the sample.

On the bottom of the vacuum volume, various materials were placed predominantly in the form of thin discs with a diameter of 95 mm. By using a magnetic sweep, the materials were uniformly irradiated by a 2 MeV proton beam with a current of 500 μ A. With the help of a web-camera, the surface of the sample was monitored, as was, in some cases, the uniformity of scanning of the beam pattern when heated. The absorbed dose of electromagnetic radiation was measured using a spherical ionization chamber at a distance of 25 cm from the center of the sample, and neutron radiation dose was measured by a DKS-96 dosimeter-radiometer with a BDMN-96 detection unit at a distance of 50 cm. Since in the readings of the ionization chamber is a certain contribution of Bremsstrahlung radiation from the accelerator, to determine this contribution, the readings of another ionization chamber located at a large distance from the irradiated samples which measured the radiation only from the accelerator were used. It was determined that the dose rate increases linearly with increasing current. Table 7 shows the dose rates per unit current for all materials calculated by the least squares method with the use of linear approximation of experimental data. In addition, we draw attention to high radiation power from barium fluoride and lithium fluoride crystals. To eliminate the errors, measuring doses were duplicated using a LB6500-3H-10 gamma detector (Berthold Tech.). These crystals were irradiated with a proton beam not because they are considered as the structural materials of the target, but for experimental verification of the possibility of generating a powerful flux of positrons [109]. It is known that in the interaction of the proton with fluorine, the ^{20}Ne nucleus is formed, which disintegrates into α -particle and ^{16}O nucleus in an excited state with an excitation energy of 6.05 MeV. Excitation is removed by emission of the electron-positron pair. This reaction is written in the form $^{19}\text{F}(p, \alpha e^+ e^-)^{16}\text{O}$. Its cross section reaches a value of 0.2 b at a proton energy of 2 MeV. Figure 14 shows the spectrum of γ -radiation upon absorption of protons with an energy of 2 MeV in barium fluoride. The spectrum was measured using a BGO γ -spectrometer (the scintillator has a diameter of 80 mm and a height of 100 mm) located under the vacuum volume. One can clearly see the γ -quanta with an energy of 511 keV born as a result of the positron annihilation. This property of generating intense γ -quanta flux can be

Table 6. Dependence of γ -quanta yield on the proton energy and the thickness of lithium

Proton energy, MeV	γ -Quanta yield for 10 mA proton beam, s^{-1}	
	thick target	thin target
2.5	3.5×10^{12}	2.2×10^{12}
1.915	1.4×10^{12}	1.4×10^{11}
1.77	6.3×10^{11} [108]	0

Table 7. Absorbed dose of γ -radiation under irradiation of materials by protons with an energy of 2 MeV

Material	Dose rate, $\mu\text{Sv/h m}^2 \text{ mA}$	The accuracy of determining the dose rate, %
Lithium (Li, 50 μm)	750	5
Graphite (C)	25	10
Lithium fluoride (LiF)	20000	20
Barium fluorid (BaF_2)	6500	20
Aluminum (Al)	150	5
Silicon (Si)	23	2
Titanium (Ti)	230	8
Vanadium (V)	270	4
Stainless steel (Fe, 12X18H10T)	70	10
Copper (Cu)	90	5
Molybdenum (Mo)	<6	
Tantalum (Ta)	<6	

used for diagnostics of current or a current profile of the proton beam, for example, by measuring the dose of γ -radiation when introducing a sample with fluorine into the beam.

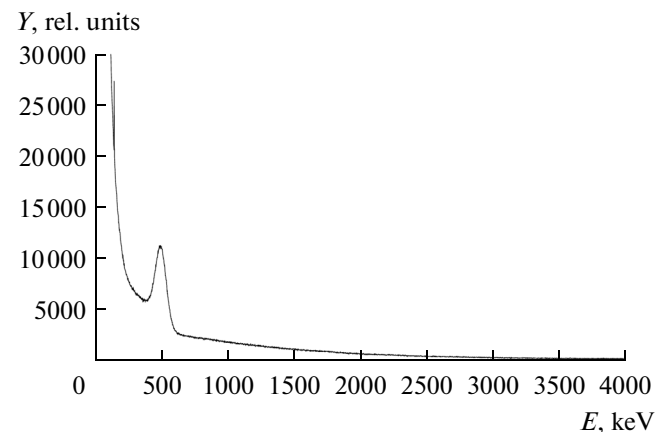


Fig. 14. The spectrum of γ -radiation under irradiation of barium fluoride with the proton beam with an energy of 2 MeV.

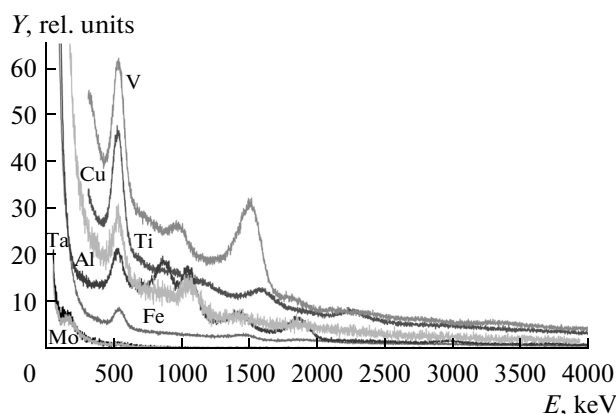


Fig. 15. Gamma radiation spectra of materials irradiated by a proton beam with an energy of 2 MeV: vanadium (V), titanium (Ti), copper (Cu), aluminum (Al), stainless steel (Fe), tantalum (Ta), molybdenum (Mo).

Figure 15 shows the spectra of gamma-radiation upon absorption of 2 MeV protons in structural materials, measured using a BGO γ -spectrometer. The proton absorption in lithium leads to the generation of a monochromatic γ -quanta flux with an energy of 478 keV. The corresponding experimental results are presented in [81]. Figure 15 shows that radiation from molybdenum and tantalum is almost completely absent.

A noticeable residual activity is detected on graphite, titanium, and lithium fluoride. It was determined that graphite activation occurs due to the process $^{12}\text{C}(p)^{13}\text{N} \rightarrow \beta^+ (10 \text{ min}) \rightarrow ^{13}\text{C}$; the activation of titanium is due to the proton absorption by the ^{46}Ti and ^{47}Ti isotopes that is accompanied by the decay of the ^{47}V , ^{48}V nuclei, and the electron capture of ^{48}V [13]; and activation of lithium fluoride occurs due to the production of radioactive ^7Be isotope in reaction $^7\text{Li}(p,n)^7\text{Be}$. Activation of titanium using a proton beam can also be used to measure the charge transferred by the beam.

It was found that irradiation of stainless steel, titanium, and vanadium using the proton beam at an energy of 2 MeV leads to the neutron yield. The absorbed dose was measured by a DKS-96 dosimeter-radiometer. For vanadium it equals $7000 \mu\text{Sv}/(\text{h m}^2 \text{ mA})$, and is 25 times less for stainless steel. Generation of neutrons is confirmed by the presence of a characteristic signal of detector caused by reaction $^6\text{Li} + n \rightarrow ^3\text{H} + \alpha + 4.785 \text{ MeV}$. The detector contains lithium-GS20 scintillator 18 mm in diameter, and 4 mm in thickness (Saint-Gobain Crystals, USA). Figure 16 shows the dependence of the counting rate of the detector in the region of the neutron peak as a function of the proton energy. These data allowed one to determine that the generation of neutrons from stainless

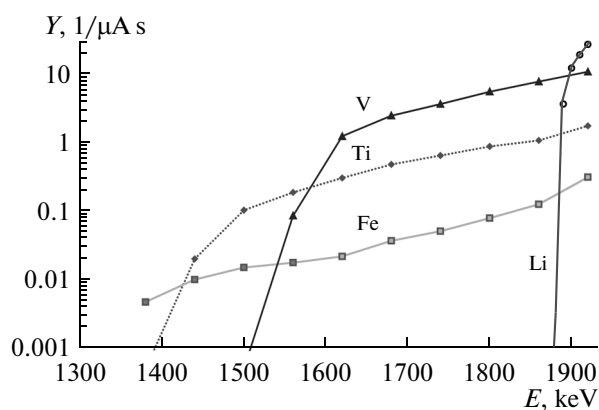


Fig. 16. The counting rate of the neutron detector in the neutron peak as a function of the proton energy during their absorption in vanadium (V), titanium (Ti), stainless steel (Fe), and lithium fluoride (Li).

steel occurs via the reaction $^{55}\text{Mn}(p,n)^{55}\text{Fe}$ (1.034 MeV reaction threshold) owing to the presence of manganese as an impurity, reaction $^{49}\text{Ti}(p,n)^{49}\text{V}$ (1.43 MeV reaction threshold), vanadium, and reaction $^{51}\text{V}(p,n)^{51}\text{Cr}$ (1.562 MeV reaction threshold). Since the threshold of these reactions is significantly lower than the threshold of the $^7\text{Li}(p,n)^7\text{Be}$ reaction, the energy of neutrons in this case is higher than the energy of neutrons emitted from lithium. For this reason, the application of these structural materials—stainless steel, titanium and vanadium—as the substrate neutron-generating targets is undesirable. The point is that the beam shaping assembly is optimized for moderation of neutrons emitted in the $^7\text{Li}(p,n)^7\text{Be}$ reaction. It cannot provide an appropriate deceleration of fast neutrons. As a result, an additional dose of unwanted fast neutrons appears during treatment.

Thus, it was found that absorption of 2 MeV protons in the molybdenum or tantalum is accompanied by the minimal dose of rays and γ -radiation and does not lead to the generation of fast neutrons and residual activity. Previously it was determined that tantalum, vanadium, and α -iron have a maximum resistance against the radiation damage (blistering) upon the absorption of protons with an energy of 2 MeV and a material temperatures of about 150°C . Thus, it was found that the optimal substrate material for lithium neutron-generating target for BNCT with minimum flux of unwanted radiation and maximum resistance to radiation damage proves to be tantalum [110].

VACUUM DEPOSITION OF LITHIUM LAYER

Figure 17 shows the scheme of the system designed and manufactured for vacuum deposition of lithium onto the substrate of the target. An industrially manufactured plate valve was used upon this fabrication.

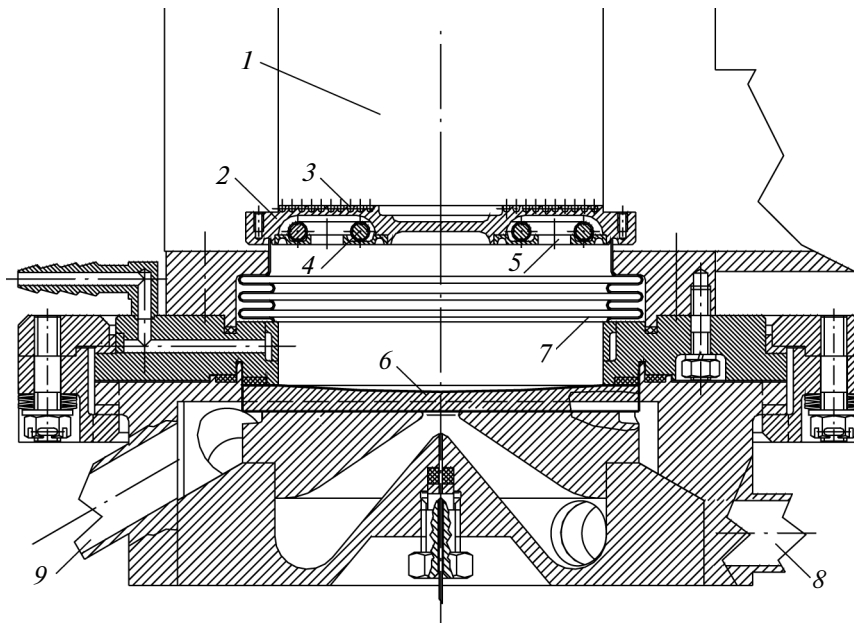


Fig. 17. Neutron-generating target with lithium deposition system: 1—proton tract, 2—plate of the gate, 3—heater mounted on the plate of the gate, 4—container with lithium, 5—circular outlet for vaporized lithium, 6—beam receiver onto which lithium is deposited, 7—bellows, 8 and 9—cooling water feed and drainage.

Heater 3 is placed on the plate of valve 2, and vaporizer with circular slit 5 is placed beneath the plate, inside of which lithium container 4 is installed. Before the deposition, the valve disc moves into the proton tract and shifts in the direction of the target by 5 mm, using the mechanism of the valve seal. As a result of the shift, the plate is pressed against bellows 7, which limits the amount of deposition. Then, the heater is switched on and vapors of lithium are distributed through circular slit 5. As the bellows is thermally insulated and heated during the process of deposition, the deposition on the bellows does not occur. Deposition is carried out only onto target substrate 6, which is water cooled.

Testing of the deposited layer on the lithium target was performed at the vacuum test bench. Before depositing, lithium containers are placed into the heater [111]. The containers represent hollow thin-walled closed aluminum enclosures filled with pure lithium. The fabrication procedure of lithium containers is as follows. Pure lithium (in sufficient amount) is stored inside a specially manufactured bellows in the robust housing. The volume between the bellows and enclosure is filled with oil. The oil pressure is raised by means of the plunger pump, the bellows is compressed, and lithium pressurizing the plug escapes through the nozzle in the form of a wire with a diameter of 4 mm. Lithium wire is cut into pieces and is wrapped tightly in an aluminum foil. Aluminum foil prevents the interaction of lithium with air and eliminates the need to work in an inert atmosphere for loading the lithium into the heater. After loading of the container with lithium into the valve plate and pump-

ing out to 10^{-5} Torr, the heater is switched on. It is found that for lithium evaporation the container should not be heated to the melting point of aluminum 660°C : it is sufficient to heat to lower temperatures, for example, to 460°C . Most likely, lithium reacts with aluminum upon heating, and this alloy melts at a lower temperature. Since at this temperature the pressure of aluminum vapors is about 10^{-12} Torr, and lithium is 10^{-3} Torr, then only lithium evaporates. Vapors of lithium go out through the circular hole with a diameter of 7 cm and a width of 0.6 cm that was cut beneath the damper plate (5 in Fig. 17), and are deposited onto a cooled substrate of the target.

To measure the radial distribution of thickness of the deposited layer of lithium, a new methodology was proposed. The necessity of this proposal is related with the fact that, first, lithium is a very active metal and instantly forms the compounds in air, and secondly, many standard measurement techniques in vacuo are inapplicable because in the vicinity of the cooled target an evaporator with high temperature is placed. So, it is impossible to use the method of determining the mass of lithium sputtered onto piezoceramics by measuring the resonance frequency of the ceramics, since the deposition process for ceramics is significantly different from the deposition onto the cooled copper substrate due to different temperatures.

The essence of the proposed method is to measure the electrical conductivity of the distilled water in which the lithium layers sputtered on thin precursors of the same material as the target are dissolved; these are in good thermal contact with the target during

sputtering. The obvious advantage of this method, as was established, is that the electrical conductivity of water depends only on the mass of dissolved lithium and does not depend on whether the lithium is in pure form or it is a part of any compound (hydride, lithium oxide, or nitride). The measurements were carried out using a commercially fabricated device: an Anion 410 ion-conductivity meter.

To determine the lithium layer thickness, thin copper plates (“bystanders”) were laid in the form of two crossed rows onto the cooled target 10 cm in diameter with a surface of 1 cm^2 , which have a good thermal contact with the target through the indium-gallium connection. It must be noted that if the “bystander” is simply laid on the surface, a thicker layer is deposited due to higher temperature of the “bystander.” After vacuum deposition, the working volume is filled with air. The target onto which the lithium has been deposited is removed, and the “bystanders” are placed in water. The amount of lithium deposited on the “bystander” is measured via the water conductivity. It was found that the measured thickness distribution of the lithium layer is in good agreement with simple calculation of collisionless scattering of lithium vapor from the circular hole. The thickness of lithium measured by this technique turned out to be in a good agreement with the results of direct micrometric measurements. This means that the density of the deposited lithium layer corresponds to the density of crystalline lithium (0.54 g/cm^3) [112].

At the accelerator in Birmingham, a decrease in the neutron yield by 10% was earlier found after 3 h of operation and a dump of 2.8 MeV 1 mA proton beam onto the lithium target with a thickness of 1 mm and a diameter of 40 mm [113]. It was assumed that the possible reason for this could be the change in the composition of lithium layer as a result of its interaction with residual gas, since the neutron yield, for example, from lithium nitride, is smaller by factor of 1.66 than that of pure lithium.

Using the mass spectrometry of secondary ions, the distribution of elemental composition across the thickness of lithium layers exposed in various vacuum conditions was measured. To transfer the samples deposited by sputtering to a MIQ-256 setup of the secondary ion mass spectrometry (CAMECA-RIBER, France), a special device with argon blowing was developed to prevent lithium interaction with an atmospheric air. The studies allowed one to determine that an experimentally observed decrease of the neutron yield at the accelerator in Birmingham is not associated with the interaction of lithium with residual gas. By using the mass spectrometry of secondary ions it was found that the purity of the lithium layer and its resistance to the residual gas is sufficient for effective neutron generation [114].

PROTECTIVE CONTAINER (IN A DEPTH) FOR HOLDING AND TEMPORARY STORAGE OF ACTIVATED TARGETS

One of the problems to be solved is associated with the target activation as a result of reaction ${}^7\text{Li}(p,n){}^7\text{Be}$. Generation of neutrons in this reaction is accompanied by the accumulation of radioactive ${}^7\text{Be}$ isotope in lithium layer. Efficient heat removal [97] makes it possible to maintain the layer of lithium in the solid state (below the melting point of lithium) when it is heated by a proton beam. Thus, the retention of radionuclide in the lithium layer and the absence of its spreading throughout the installation are provided. After achieving a certain magnitude of activity which prevents the conduction of experiments or therapy, or the target operation limit by exposure to the proton beam radiation, it is supposed to remove the target and displace the part of the target, namely the beam receiver with lithium layer (6 in Fig. 17) into the protective container for decontamination. This procedure seems to be optimal, because on the one hand, the half-life of ${}^7\text{Be}$ (53.3 days) is not too large to implement a simple possibility of deactivation of the target in container in a natural way. On the other hand, this period is too long to perform short-term operations for removing the target from installation and placing it into container.

Two modes of neutron generation are used in the setup: standard mode with a proton beam energy of 2.5 MeV, and near-threshold mode with an energy of 1.915 MeV. In the first case, the neutron yield is $8.9 \times 10^{12} \text{ s}^{-1}$ at a proton current of 10 mA, and it is almost 30 times less in the second case [31]. From the standpoint of the target activation, the worst mode of the neutron generation is at an energy of 2.5 MeV, which we will consider. Each neutron is associated with the formation of the ${}^7\text{Be}$ nucleus, which is transformed with a half-life of 53.3 days into the stable ${}^7\text{Li}$ nucleus. In 10.3% cases, the decay is accompanied by the photon emission with an energy of 0.4776 MeV [116]. To evaluate the target activation, we assume that the source generates the neutrons not around the clock, but only 1/10 of the time, which seems to be quite realistic and even hardly achievable. The beryllium formation occurs with a time scale of 77 days and after a year the activity of ${}^7\text{Be}$ reaches a stationary value of $8.9 \times 10^{11} \text{ Bq}$, numerically equal to the rate of generation of neutrons at an average current of 1 mA. At such activity the target emits 9.2×10^{10} photons per second with an energy of 0.4776 MeV. The calculated kerma of ${}^7\text{Be}$ (in air) equals $1.86 \times 10^{-18} \text{ Gr m}^2/(\text{s Bq})$ [117]. The saturated value of kerma-equivalent of ${}^7\text{Be}$ after a year equals $6 \times 10^3 \mu\text{Gr m}^2/\text{h}$. At a distance of 2 m from the point source with such an activity, which is not surrounded by any other materials, the kerma rate is equal to $1.5 \times 10^3 \mu\text{Sv/h}$. In areas of temporary stay of personnel, the design equivalent dose for standard

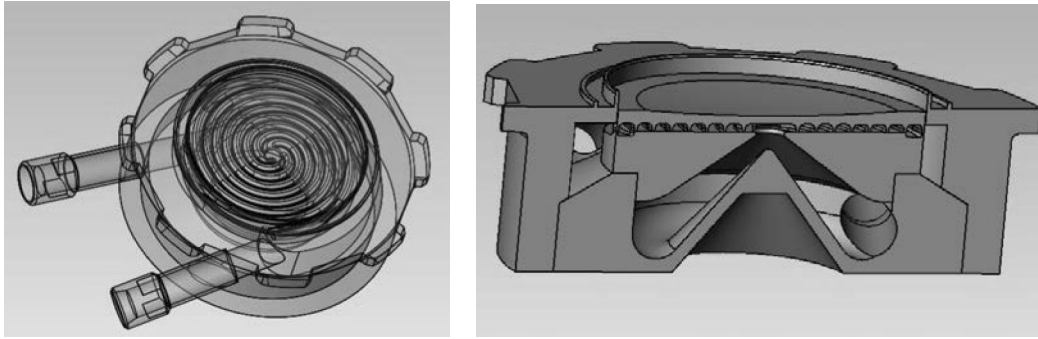


Fig. 18. Isomeric view of the target unit with beam receiver.

conditions, in accordance with OSPORB-99 [118], is $12 \mu\text{Sv/h}$. Neglecting small (in our case) difference between the corresponding numerical values of the equivalent dose rate and the air kerma, one can see that we need to reduce the kerma by about 125 times. In accordance with universal data tables by Mashkovich and Kudrjavitseva [117] (Tables 5.41 and 5.43), such weakening of an isotropic point source in an infinite medium can be achieved by using a 3 cm of lead or 40 cm of concrete.

It has been proposed to fabricate the container for holding and temporary storage of activated targets in the form of long steel cartridge embedded in the ground, with an inner diameter of 219 mm and a height of 2 m, on the bottom of which (the bottom thickness is 10 mm) the activated targets are placed. A cartridge is covered with a lid on the top, which is a sandwich of a steel disc with a thickness of 10 mm and a diameter of 280 mm (by 60 mm larger than the outer diameter of the pipe), and a thick disk of lead mounted on it, the final thickness of which to be taken after further calculations. Design of the cover should provide sealing to avoid the inlet of moisture and heavy inert gas, if necessary. A feature of the proposed configuration of container is that onto the protective cover (on the bottom), in addition to direct flux of photons with an energy of 0.4776 MeV from the targets, a significant amount of radiation comes from being scattered by a steel wall of the container tube and the adjacent ground. In addition, multiply scattered radiation flux of the soil coming out of the floor surface in the immediate vicinity of the perimeter of the protective cover can also exert a significant influence on the formation of the radiation field above the container. In this situation, the results of simple preliminary estimates of protective requirements which were obtained using the universal tables by Mashkovich and Kudrjavitseva [117] seem to be insufficiently correct. To adequately account for the geometric features of the proposed variant of container, the simulation of gamma-radiation transport was carried out using the PRISMA program and Monte Carlo method [115]. For this pur-

pose, the radial distribution of dose above the container at a height of 0.5 m from the floor for four values of the thickness of the disc, namely 30, 40, 50, and 60 mm, was computed [119]. It is found that the lid of the container with a lead disk of 50 mm thickness would allow researchers to retain the dose rate at a level no more than $2 \mu\text{Sv/h}$, which is acceptable. A technical project for the container and temporary storage of activated targets was developed and coordinated on the basis of the calculations. In the bottom room of the hopper in which the accelerating neutron source was mounted, a hole was made in the concrete floor, and a dimple was drilled in which the tube with welded bottom was inserted. Free space around the pipe was closed by the soil and concreted on the top. The pipe was installed with slight elevation above the floor and was closed by the lid. The warning system was mounted on the opening of the lid and the fence was set. As a result, creation of such protecting container for holding and temporal storing of activated targets makes it possible to solve the problem of the target activation being necessary in long-term generation of neutrons [119].

CONSTRUCTION OF THE NEUTRON-GENERATING TARGET

Using the results of the studies, a neutron-generating target was fabricated [93, 120] which is currently used to generate neutrons. Since this system is combined with the system of lithium deposition, its general and isomeric schemes are shown in Figs. 17, 18. An important element of the target is the beam receiver with thin lithium layer deposited. The beam receiver is made of copper in the form of a disk with a diameter of 122 mm and a maximum thickness of 8 mm (proton beam irradiates the surface with a diameter of 100 mm). A spherical recess of 2 mm depth was made in the disc from the side of the proton beam with a radius of 626 mm to prevent the deformations under the action of pressure of cooling water. Four spiral channels with a depth of 3 mm and a thickness of 6 mm were made from the back side. The beam



Fig. 19. Photo of the target unit and beam receiver.

receiver is tightly pressed to the enclosure of the target. The cooling water is introduced tangentially into the inner cavity of the body of the target, is unwound as the cyclone, is sent into the channels of beam receiver through the aperture in the center, and then flows outwardly along the bifilar spiral channels. At a pressure of 2 atm of distilled water at the inlet channel of the beam receiver, a turbulent flow of water is implemented (Reynolds number 4×10^4) with a speed of 10 m/s to provide the desired heat removal and to keep the lithium layer in the solid state up to 25 kW of heating power. In this case, the water consumption equals $3.5 \text{ m}^3/\text{h}$, and the water is heated by 8°C .

The target unit is made of a stainless steel and is attached to the installation by means of a bayonet connector (Fig. 19). The bayonet connector allows one to quickly remove the target unit, by turning it to release the beam receiver with lithium layer. Simplicity and rapidity of the substrate release is required to minimize the dose obtained by personnel when removing the beam receiver activated by berillium-7 after neutron generation and placing it inside the closed recessed container for holding and temporal storing.

The results obtained in the development of neutron-generating target were used in many projects in their manufacturing. At the KURRI (Osaka, Japan) cyclotron neutron source, the beam receiver exactly duplicates the source developed in [121, Fig. 3]. In the American project of linac, the target is modified in the form of the cone [122]. In the project of the IBA Co., the target consists of two inclined plates [53], and of one inclined plate in the Korean project [123]; all the projects have nearly same parameters.

THE BEAM SHAPING ASSEMBLY

Despite the fact that the ${}^7\text{Li}(p,n){}^7\text{Be}$ reaction allows one to generate the softest spectrum of neutrons, it is necessary to moderate them for the use in BNCT. Ideally, the neutrons should have the energies in the range of 10 keV. To form therapeutic neutron beam, the beam shaping assembly is used (BSA), comprising a moderator, reflector, absorber, and filter (in some cases). Over the last ten years, a possibility of manufacturing lithium target has become apparent. For the ${}^7\text{Li}(p,n){}^7\text{Be}$ reaction, BSA has been optimized by several research groups using the proton beams with energies from 2.3 to 2.8 MeV [124–132]. At the same time, standardization of the calculations has occurred (for their comparison). As the phantom, wherein the transport of neutrons, γ -quanta and their doses were calculated, almost all researchers began to use the modified Snyder head phantom [133]: three ellipsoids nested one into another with different compositions of elements which are as close as possible to the compositions of skin, bones, and brain. In the calculations, the values of relative biological effectiveness (RBE) are used [134]. For brain tissues, RBE equals 1.0 and 3.2 for photons and neutrons, respectively. The combined biological effectiveness (CBE) equals 1.35. For tumor, RBE is the same, while CBE is equal to 3.8.

When calculating doses for the modified Snyder phantom, the following processes are taken into account. The first is the process of neutron absorption by boron with the energy release of 2.79 MeV. In 6.1% cases, the energy is distributed only between the nuclei of lithium and α -particle; in 93.9% cases the lithium nucleus is emitted in an excited state and emits γ -quantum with an energy of 0.48 MeV. The second process is the neutron capture by the nuclei of hydrogen,

leading to the formation of deuterium and the emission of γ -quantum with an energy of 2.2 MeV. Third is the occurrence of recoil protons from the interaction of predominantly fast neutrons with nuclei of matter, preferably hydrogen, and absorption of neutrons by the nuclei of nitrogen with an energy release of 580 keV. The γ -quanta flux is taken into account rather frequently, but the dose caused by the neutron absorption in chlorine is nearly always neglected due to its smallness. Thus, the following components of doses are separated from all the processes, including those quanta which arise under neutron absorption by boron and hydrogen and those which escape from the target, the system of beam formation, and other constructions: (1) so-called "boron" dose (from α -particles and lithium); (2) fast neutron dose (from recoil protons under elastic neutron scattering); (3) dose from neutron absorption by nitrogen (also as a result of production of recoil protons), and (4) dose of γ -quanta.

It was found that the moderator should be made of material with the highest concentration of fluorine because only fluorine has a significant inelastic neutron scattering cross section at energies below 1 MeV, which provides rapid moderation of neutrons to energies of about 100 keV. Of course, the hydrogen moderator also effectively reduces the energy of neutrons, but the neutron spectrum formed is largely shifted to thermal energies and it is impossible to obtain perfect narrow spectrum of energies from 1 to 30 keV with the use of such neutrons. An optimum moderator may be made of magnesium fluoride, lithium fluoride and aluminum fluoride, or PTFE (polytetrafluorethylene). Lead and graphite are used for the reflector. The absorber may be polyethylene with the addition of boron or lithium. Such BSA for a proton beam with an energy of 2.5 MeV and a current of 10 mA provides a dose rate of 1 Gy/min, the depth of treatment provides up to 10 cm, and therapeutic ratio provides up to 6. This is acceptable for BNCT.

This mode of neutron generation in the reaction ${}^7\text{Li}(p,n){}^7\text{Be}$ at a proton energy of 2.5 MeV was also computed by us. Numerical simulation of the transport of protons, neutrons, and gamma-radiation was carried using the Monte Carlo program PRISMA [135], the database of ENDF/B-VI cross sections and the constants from reference book [136]. As in the above calculations, the therapeutic neutron beam and proton beam are collinear. This geometry will be called "standard." Figure 20 shows a schematic diagram of the BSA, and Fig. 21 displays the neutron spectrum. The depth distribution of dose is shown in Fig. 22, and Fig. 23 shows the total dose distribution in the modified Snyder head phantom. In the calculations, the concentration of boron-10 in a healthy and tumor tissue was assumed to be 15 and 52.5 ppm, respectively. One can see that the results obtained are similar to those described above, namely a dose rate of 1.5 Gy/min, a therapy depth of 11 cm, a therapeutic ratio of 5, and an average neutron energy of 4 keV.

The ${}^7\text{Li}(p,n){}^7\text{Be}$ reaction is characterized by an extremely rapid growth of the cross section near the threshold, and therefore the use of near-threshold generation regime seemed to be very attractive when due to the kinematic collimation the neutron flux is directed toward and having a low mean energy of 40 keV. Despite the relative softness of the spectrum, these neutrons are not suitable for BNCT because a contribution of fast neutrons to the dose prevails, and it is necessary to moderate these neutrons. Since the neutron flux is clearly directed forward, it is required that the moderation of the neutron spectrum occurred without appreciable scattering, because the latter reduces the dose. As shown by calculations [137, 138], the use of hydrogen-containing moderator is possible, but the depth of treatment is small because of the intense neutron thermalization. The best quality neutron beam can be obtained using a set of filters. With the help of two series-mounted filters of magnesium fluoride and aluminum, the high-energy neutrons undergo scattering, while all other neutrons pass through the filters. Further, a slight moderation of neutrons occurs in polyethylene and their spectrum is shifted to lower energies. Then, the high-energy neutrons are scattered again using the aluminum filter, and the final formation of the right wing of the spectrum is performed by means of the titanium filter. Thus, the scattering of high-energy neutrons allows one to create a softer neutron spectrum without significant loss in the flux. In [139], the authors presented the calculation results corresponding to the following geometry. Moderator filter with a thickness of 46 mm was placed directly behind the target and has been made of 6 layers ${}^6\text{Li}$ (1 mm), MgF_2 (6 mm), Al (9 mm), C_2H_4 (16 mm), Al (9 mm), and Ti (5 mm). The target and proton transport line were surrounded by the graphite reflector with a thickness of 50 mm, and the absorber of borated polyethylene had a thickness of 50 mm with lead cylinders of 10 mm thickness. The obtained dose rate was equal to 1 Gy eq/min, the depth of treatment was 7 cm, and the therapeutic ratio was 2.5. Although all these parameters are below those in the standard mode, the near-threshold mode has the advantage that it effectively uses the generated neutrons: namely the neutron yield is 10 times smaller than in the standard mode, while the dose is smaller by only 1.5 times.

The best quality therapeutic neutron beam can be obtained using the neutrons emitted perpendicular to the protons as they initially have a softer spectrum than in the standard mode. By turning the moderator by 90° and having surrounded it by reflector (Fig. 20), we obtain an increase in the dose rate by 2 times, up to 3 Gy/min, and the depth of treatment increases up to 12 cm, but with the simultaneous deterioration of the therapeutic ratio up to 4. This change is due to a harder neutron spectrum, since their average energy increases up to 14 keV. Due to a harder spectrum, the dose rate has grown in normal tissues on the surface of skin and reached a maximum value (in a depth). However, the

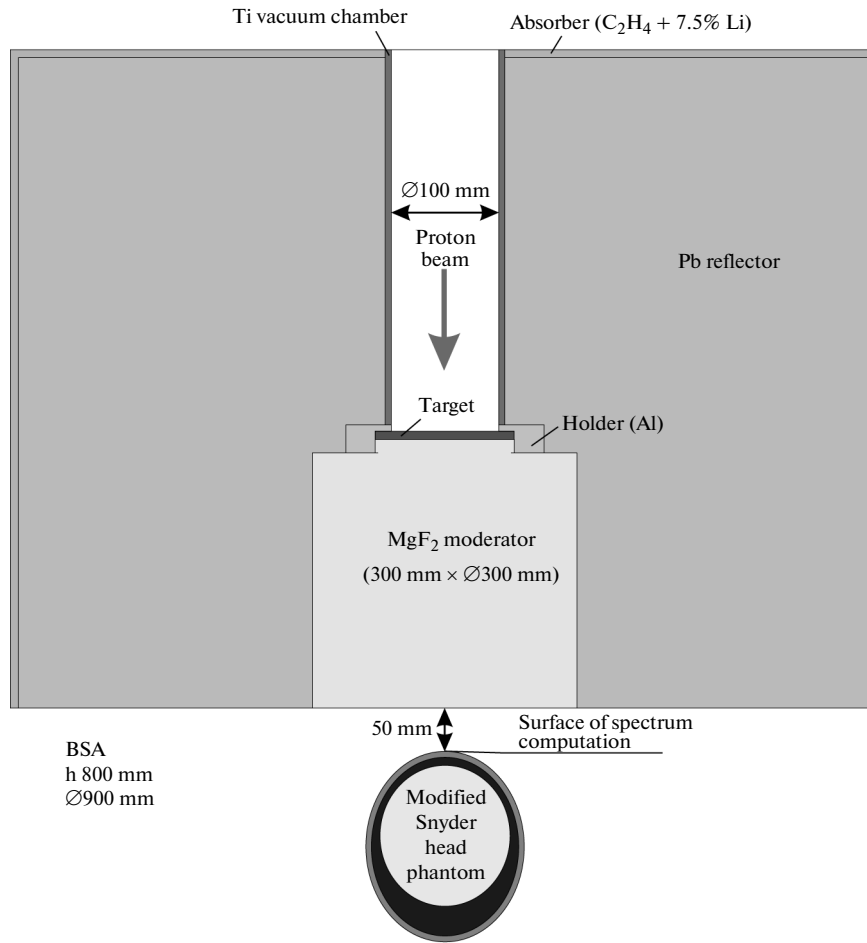


Fig. 20. Beam Shaping Assembly (BSA).

orthogonal mode brings a new quality to the therapy, allowing technicians to perform the exposure of a patient at any angle by simply rotating the BSA (Fig. 24), i.e., irradiating different areas of skin and

thus improving the therapeutic ratio. Also, this system makes it possible to direct neutrons under such an angle at which the therapy of specific tumor gives the maximum effect [140].

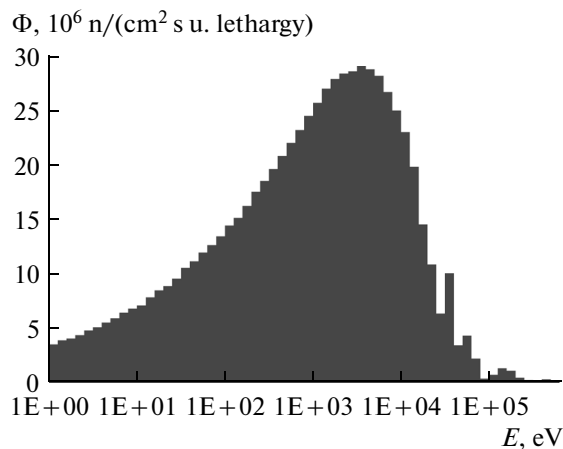


Fig. 21. Calculated neutron spectrum.

GENERATION OF NEUTRONS

Neutron production occurs when dumping the proton beam onto the lithium target. The neutron yield was measured by two methods [81, 141]. In the first method we used the fact that the production of each neutron in the reaction ${}^7\text{Li}(p,n){}^7\text{Be}$ is accompanied by the formation of radioactive ${}^7\text{Be}$ nucleus with a half-life of 53 days. The total neutron yield was determined by the residual activity of lithium target when measuring the rate of beryllium disintegration in the target removed after the end of neutron generation and mounted above a NaI γ -spectrometer.

In the second method, the neutron activation in the NaI scintillator of γ -spectrometer was used, since epithermal neutrons are captured efficiently by the natural iodine-127 isotope (resonance integral of capture equals 140 b). The resultant ${}^{128}\text{I}$ isotope decays

with a half-life of 25 minutes. In 6.4% cases, the decay occurs due to the electron capture without any radiation; in 93.6% cases, the β^- decay occurs with the emission of an electron with an energy up to 2.12 MeV. After the end of neutron generation, the residual activation was registered, which is characteristic for the β^- -decay of nuclei of the scintillator itself. The measurements and Monte Carlo calculations of the activation rate of the NaI detector made it possible to determine the neutron yield. In both cases the experimental results are in a good agreement with the calculated [32], namely 1.1×10^{11} n/mC at a proton energy of 2 MeV.

The neutron spectrum was also measured by using two methods. The BDT and BD100P bubble detectors (Bubble Technology Industries, Canada), which are sensitive to thermal and fast neutrons, were used for primary analysis of the neutron spectrum. The number of bubbles formed in the BDT detector turned out to be 15–20 times higher than in the BD100R detector, in agreement with the calculated spectrum [141]. With a good level of details, the energy spectrum of neutrons was measured by the time-of-flight method [85] when generating short pulses of neutron radiation and neutron detection by a remote detector (Saint-Gobain Crystals) with lithium-containing scintillator GS20. To create short bursts of neutrons, a new technical solution [142] based on the use of threshold character of the cross section of the ${}^7\text{Li}(p,n){}^7\text{Be}$ reaction was proposed and implemented. The idea recalls the famous “method of flashing accelerator.” When the energy of the proton beam is below the threshold of the ${}^7\text{Li}(p,n){}^7\text{Be}$ (1.882 MeV) reaction, neutron generation does not occur. When a short (200 ns) pulse of negative voltage (40 kV) is fed to the neutron-generating target being electrically insulated from the installation [143], the proton energy is increased up to 1.915 MeV, which leads to an outbreak of neutron radiation. The measured neutron spectrum is shown in Fig. 25. An accuracy of the measurements is 5% in the range of low neutron energies and 20% at higher energies. The calculated neutron spectrum [144] is also shown in Fig. 25 for comparison.

Characteristic features of the spectrum on the graph are shown with numbers. A pronounced dip in the neutron flux in the range of 300–400 eV, marked with number 1, is associated with neutron scattering by the ${}^{55}\text{Mn}$ nuclei, which are present in the composition of stainless steel in an amount of about 2%. In this energy range, the neutron scattering cross section on the ${}^{55}\text{Mn}$ nuclei has a fairly broad peak with a maximum of 3232 b at an energy of 340 eV. Numbers 2 and 3 in Fig. 25 mark the peaks of neutron flux, which are due to free passage through the iron, since at energies of 24.5, 72.9, and 82 keV the scattering cross section of neutrons on ${}^{55}\text{Fe}$ nuclei is three orders of magnitude less than the characteristic cross sections in this energy range. It can be seen that the experimentally measured

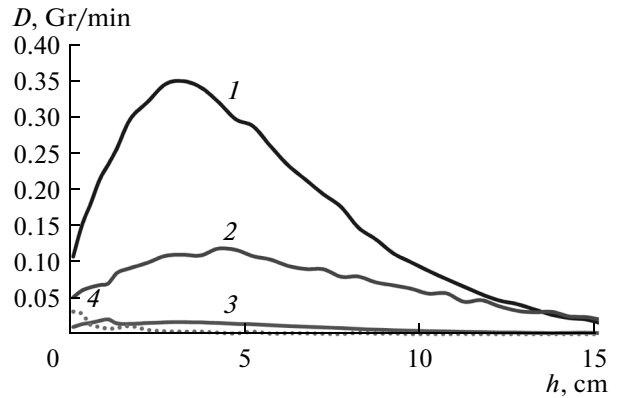


Fig. 22. Contribution to the total dose D of each of the four components as a function of the depth h in the modified Snyder head phantom: (1) as a result of reactions ${}^{10}\text{B}(n,\alpha){}^7\text{Li}$ at the ${}^{10}\text{B}$ concentration of 52.5 ppm, (2) from γ -rays, (3) as a result of reactions ${}^{14}\text{N}(n,p){}^{14}\text{C}$, (4) as a result of neutron elastic scattering.

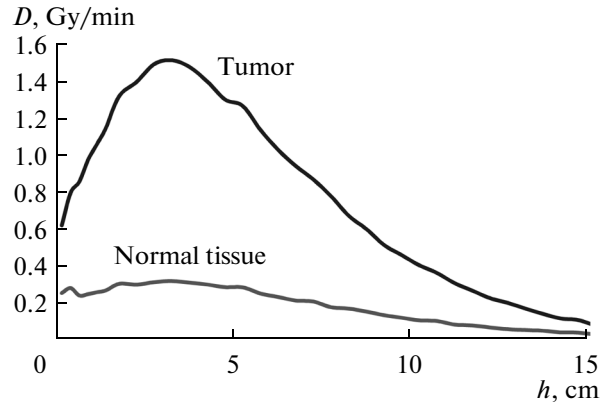


Fig. 23. Total doses D in the tumor and in normal tissue as a function of the depth h in the modified Snyder head phantom.

spectrum agrees well with the calculated one, excluding a range of 1 to 20 keV. The measured neutron flux has an average energy of 13 keV and even better corresponds to the “ideal spectrum” of neutrons for BNCT [7, pp. 43 and 65] than the calculated spectrum.

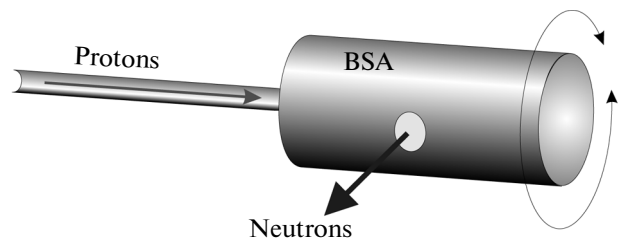


Fig. 24. Orthogonal beam shaping assembly with the possibility of rotation.

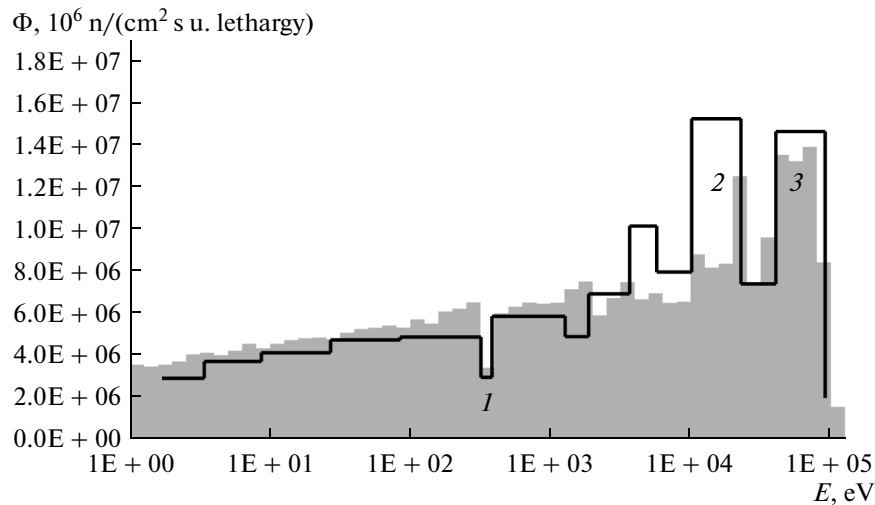


Fig. 25. The measurement results of the neutron spectrum: the columns show the calculated spectrum of neutrons, the line shows the measured spectrum, the numbers 1–3 indicate the characteristic features of the spectrum.

Measurement of spatial distribution of the dose rate of neutron radiation was measured using a DKS-96 dosimeter-radiometer with a BDMN-96 detection unit. It was determined that the dose rate decreases with the distance squared and has a small permanent value related to the contribution of the reflected neutrons. The measured value of the dose rate is about 2.5 times higher than the calculated, which may be associated with a relatively soft spectrum of the generated neutrons. For the same reason, one obtains even higher readings using a DVGN-01 individual dosimeter of mixed radiation [146, 147]. Measurement of the angular distribution of the dose rate confirmed the directionality of neutron flux: the dose rate in the direction of 35° is reduced by 13% and by 2.7 times in the direction of 90° to within 10% accuracy.

Measurement of spatial distribution of gamma-radiation was carried out using a pair of γ -detectors LB6500-3H-10 (Berthold Technologies, Germany). In this case, the dose also decreases with distance squared and has a small permanent value related to the contribution of bremsstrahlung from the accelerator. But in contrast to the measurement of the neutron dose rate, the measured dose rate of γ -radiation agrees well with the calculated one. It is important to note that the contribution of γ -radiation from the target is about 1/60 of the calculated dose in the tumor. Thus, a thin lithium neutron-generating layer reduces the contribution of an undesirable γ -radiation from the target to an acceptably small magnitude.

INVESTIGATION OF THE EFFECT OF NEUTRON RADIATION *in vitro*

The effect of epithermal neutrons on the viability of tumor cells has been studied at the set up using the cell

line of human glioblastoma U87. Analysis of the cell viability after irradiation was carried out using specific staining with trypan blue, and the flow cytometry was studied using propidium iodide. An increase in the number of dead cells with increasing dose of neutron radiation was established. It is shown that the effect of neutrons on the cells of human glioblastoma U87 leads to their death, probably by increasing the apoptotic process [148]. Then, the investigation was repeated, with the difference that a part of the U87 cells were enriched with boron by incubation in the medium of boron-phenylalanine enriched with boron-10 isotope, the former being in an optically isomeric form L (BPA). The test samples were placed in the phantom of plexiglas at a depth of 3 cm and on the surface, and subjected to neutron irradiation. Analysis of the clonogenic cells and investigations with the use of staining by Hehst showed that after two weeks after irradiation, the phantom cells placed inside the phantom without boron were hardly damaged, but all the cells with boron were killed [149]. This fact clearly demonstrates the effect of BNCT selective destruction of cells enriched with boron-10. The cells without boron, placed on the surface of the phantom, were partially damaged because of the larger dose of fast neutrons. The fact that the part of cells with boron placed on the surface of the phantom has survived is explained by the smaller dose due to the resulting lower density of thermal neutron flux.

BNCT ACTIVITY PLAN

As shown earlier, the highest quality of therapeutic neutrons can be obtained with an orthogonal beam formation system at an energy of the proton beam

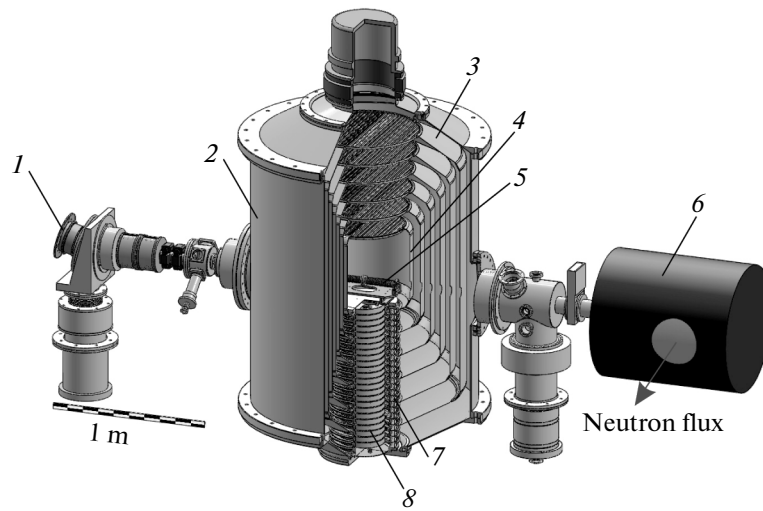


Fig. 26. Design of the neutron source for BNCT: 1—source of H^- , 2—accelerator, 3—intermediate electrodes, 4—a high-voltage electrode, 5—stripping target, 6—BSA, 7—isolator, 8—high-voltage power supply.

from 2.3 to 2.5 MeV. The beam current required for therapy for one hour should be not less 3 mA. To achieve the required parameters of the proton beam (energy increase by 20% and current increase by 2 times) and formation of neutron flux that satisfies the requirements of BNCT, the following works are planned. First, the replacement of glass vacuum rings of the bushing by the rings of polycarbonate was prepared, which are characterized by the developed outer surface, in order to increase high-voltage strength of vacuum gaps. Second, to increase the proton beam current, it is supposed to improve the vacuum conditions by installing a cryogenic pump at the accelerator entrance and upgrading the stripping gas target, and also by replacing the source of negative hydrogen ions by new source with higher current, already constructed and tested. Third, the neutron-generating target will be replaced by a new thin tantalum target with remote system for lithium layer deposition. Fourth, the beam shaping assembly will be fabricated, protected by RF patent [150]. Implementation of these works will allow researchers to come closer to the carrying out BNCT on the setup.

In order to construct a truly compact accelerator neutron source for BNCT, it is suggested to integrate the high-voltage power supply inside the tandem accelerator with vacuum insulation [151, 152]. The use of modern element base will allow researchers to fabricate sectional rectifier which is significantly smaller than that shown in Fig. 5, and mount it inside the insulator. Figure 26 shows the design of the new compact medical setup.

MONOENERGETIC NEUTRON SOURCE

Currently, a number of experimental observations—namely rotation curves of galaxies [153], grav-

itational lenses [154], temperature fluctuations of relict radiation [155], and an abundance of light nuclei [156]—point to the possible existence of “dark matter” constituting the bulk of the universe. Most suitable candidates to explain totality of the data are considered to be weakly interacting particles (WIMPs) [157]. These nonrelativistic particles represent the particles of cold dark matter, their mass lies in the region of 10 GeV, and they can be found since the Earth moves relative to the center of the galaxy, and cold dark matter is thought to be motionless. There are currently some signals registered by different detectors which may be associated with the ionization of atoms of detection medium caused by the interactions with WIMPs [158–160]. Since the solar system revolves around the center of the galaxy at a speed of 220–250 km/s, and the Earth revolves around the Sun at a speed of 30 km/s, the transferred momentum is not more than a few keV. For the interpretation of the results, it is necessary to know what part of the total recoil energy goes to ionization (quenching factor). It can be measured via the scattering of monoenergetic neutrons with energies of tens keV. Monoenergetic neutron beams used in metrology purposes overlap the range from 2 keV to 390 MeV. To obtain the neutron beams with energies of 2, 8, 24, 27, 70, and 144 keV, reactions ${}^7\text{Li}(p,n){}^7\text{Be}$ and ${}^{45}\text{Sc}(p,n){}^{45}\text{Ti}$ are primarily used, or the nuclear reactor with an iron filter is [161–163].

A method of forming the beam of monoenergetic neutrons with almost any energy was proposed in [164]. It is applicable to calibrate the detectors of weakly interacting particles with liquid argon as the working medium [165, 166]. Generation of neutrons occurs in the reaction ${}^7\text{Li}(p,n){}^7\text{Be}$ in the process of dumping of a proton beam with an energy of more than 1.882 MeV on lithium target. In the case of small

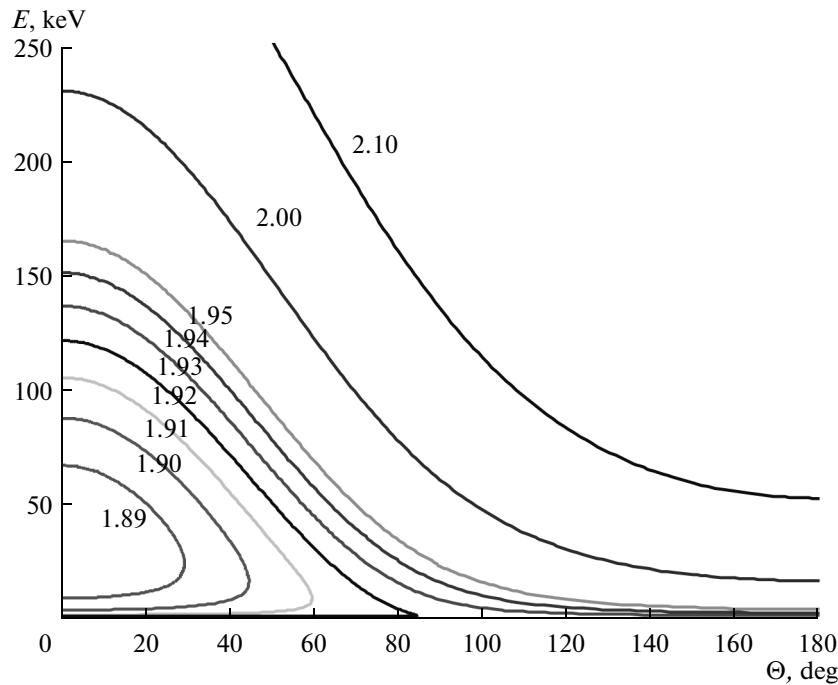


Fig. 27. Neutron energy E as a function of the emission angle Θ (in the laboratory frame) at different proton energies (MeV) indicated on curves. Angle 0° coincides with the proton beam direction.

energy change of a monoenergetic proton beam passing neutron-generating layer, the energy and the angle of neutron emission are unambiguously determined by the kinematic relations. Figure 27 shows the relationship between the neutron energy in the laboratory system of coordinates and the polar angle of emission at different proton energies [32]. One can see that at a proton energy above a threshold of 1.882 MeV, but below 1.920 MeV, the neutrons are emitted only in the forward hemisphere and are characterized by two monoenergetic lines. At proton energies above 1.920 MeV, neutrons are emitted in all directions and are characterized by only a single monoenergetic line. From Fig. 27 we can see that by varying the energy of the proton beam and an observing angle (greater than 90°), one can create a monoenergetic neutron beams with any energy. Monochromaticity of neutrons depends on the thickness of lithium layer, because the protons are slowed down when passing through it, and the energy of the emitted neutrons decreases. For example, at a thickness of $1 \mu\text{m}$ and an energy of 2 MeV, the proton monochromaticity is 2%. Monochromaticity also depends on the solid angle. At a proton energy of 2 MeV and an emission angle of 110° , 1° deg variations of the angle lead in the 2% broadening.

OTHER RANGES OF APPLICATION

Replacement of hydrogen by deuterium in the source of negative ions of the accelerator makes it possible to get the beam of deuterium, but with a slightly

lower current. By dumping a beam of deuterium onto lithium or beryllium target, a powerful flux of fast neutrons is generated, which can be used for the fast neutron therapy. This method of treatment of cancer has long been known and used, but is still not widespread for various reasons.

It was also proposed to use fast neutron flux for modifying the technique of dating the rocks containing uranium. It is known that natural uranium consists mostly of the ^{238}U isotope (abundance of ^{235}U is 0.7%), which determines radioactivity of natural uranium along with the daughter nuclide ^{234}U . As a result of spontaneous fission of uranium in rocks, tracks are formed which are visible and measurable after chemical etching. One of the methods of determining the age of rocks containing uranium is based on the comparison of the number of tracks in rocks formed over the centuries, with the number of tracks in muscovite tightly glued to the sample and irradiated by thermal neutrons along with the sample. In this case, muscovite is an external detector and allows one to visualize the tracks induced by the uranium fission. Only the fission of ^{235}U occurs under irradiation by thermal neutron flux, and one needs to have the abundance ratio of isotopes for dating the rocks. It was proposed to place the samples of uranium-containing rocks with muscovite-detector into fast neutron flux. In this case, mostly the induced fission of ^{238}U occurs, instead of ^{235}U , and information on the abundance ratio of isotopes is not required.

The inelastic scattering of protons by the nuclei of lithium leads to the generation of monochromatic γ -quanta with energies of 478 keV. Therefore, at an energy of the proton beam below the threshold of neutron generation, the setup can be a source of monochromatic γ -quanta.

The next application is associated with the development of operational methods of detection of explosives and drugs. By dumping the proton beam with an energy of 1.747 MeV onto the target of the carbon-13 isotope, the nitrogen nucleus is excited with an energy of 9.172 MeV as a result of the resonant reaction $^{13}\text{C}(p)^{14}\text{N}^*$, and the nitrogen nucleus acquires a kinetic energy of 125 keV. The excitation is removed by the γ -quantum emission, the energy of which depends on the angle between the direction of emission and momentum of the excited nitrogen nucleus due to the Doppler shift. γ -Quanta, which are emitted at an angle of $80.7 \pm 0.35^\circ$, have an energy of 9.17 MeV and can be resonantly captured by nitrogen. Thus, under the conditions of near-threshold generation, when the production of γ -rays occurs only due to the protons which changed the direction in the material, in the laboratory frame, the γ -rays resonantly captured by nitrogen are emitted at an angle of 80.7° with respect to the proton beam. The γ -quanta emitted at different angles have a slightly different energy, and they are captured by nitrogen out of resonance. Simultaneous measurement of attenuation of the γ -quanta resonantly captured by nitrogen and the nonresonantly captured quanta makes it possible to quickly identify the nitrogen-containing substance in the baggage or container. The graphite target enriched by carbon-13 isotope and the goniometer with the system of collimators have been constructed and installed. Generation of γ -quanta by damping the proton beam on the graphite target was carried out. The resonance absorption of γ -quanta with an energy of 9.172 MeV in nitrogen was measured using a BGO gamma spectrometer [82].

When passing the proton beam through the lithium, in addition to neutrons and γ -quanta, high-energy α -particles are also generated in reactions $^7\text{Li}(p,\alpha)\alpha$ and $^6\text{Li}(p,\alpha)^3\text{He}$ with an output energy of 17.347 and 4.021 MeV. The flux of α -particles is comparable to the neutron flux. In addition to the generation of α -particles in lithium target, a trial generation of α -particles in boron target was also carried out. Reaction $^{11}\text{B}(p,\alpha)\alpha$ has long been known [167, 168], but in recent years the interest in it has increased considerably because of the possibility of using it in modern neutronless fusion reactors [169]. This reaction is commonly referred to as the low-active fusion reaction, suitable for the production of fusion energy (heat) [170], and it is suitable for direct conversion of the α -particle energy into electric energy [171]. Since the accuracy of the available data on the cross section of the $^{11}\text{B}(p,\alpha)\alpha$ reaction and the spectrum of α -par-

ticles is insufficient to design the fusion reactor [172–174], accurate measurement of the reaction cross section and the spectrum of α -particles is an urgent task. These measurements can be carried out after manufacturing specialized target and the metrology system of spectrometry.

At an interaction of the proton with fluorine, the ^{20}Ne nucleus is formed, which decays into α -particle and ^{16}O nucleus in the excited state with an excitation energy of 6.05 MeV. The excitation is removed by the electron-positron pair emission. This reaction can be written as $^{19}\text{F}(p,\alpha e^+e^-)^{16}\text{O}$; its cross section is equal to 0.2 b at an energy of 2 MeV. Using the accelerator with the SF_6 gas target allows one to create a powerful source of positrons suitable for use in a number of applications, including diagnostics and measurement of the electron density in materials [109].

CONCLUSIONS

A promising method of treatment of many malignant tumors, especially incurable brain tumors, is the boron neutron capture therapy (BNCT), which is extremely attractive due to selective action directly on tumor cells. It is expected that soon a great number of accelerator sources of epithermal neutrons for BNCT will be created for the widespread introduction of this technique in clinical practice. One such source could be an original accelerator-based source of epithermal neutrons, created in BINP, to which a special attention was attracted in this work. A new type of particle accelerator—the electrostatic tandem accelerator with vacuum insulation—is characterized by high rate of acceleration of charged particles. Moreover, the isolator on which the intermediate electrodes are mounted is located far away from the path of the ion beam. The accelerator is also characterized by large energy stored in the accelerating gaps and has a strong electrostatic lens at the entrance. A stationary proton beam with an energy of 2 MeV and a current of 1.6 mA was obtained at the accelerator. The beam is characterized by the high energetic monochromaticity ($\pm 0.1\%$) and stability of current ($\pm 0.5\%$).

A neutron-generating target, optimal for the formation of epithermal neutron flux that satisfies the requirements of BNCT, was developed and experimentally investigated. The formation of an orthogonal neutron beam provides its high quality for the use in BNCT, allowing to direct the neutron beam at any angle and to irradiate the patient from all the sides.

We carried out the neutron generation and experimentally measured the neutron flux during the target activation by the ^7Be isotope and the NaI scintillator of gamma-spectrometer. The neutron spectrum was measured by using BDT and BD100R bubble detectors, and the time-of-flight method by using a new technical solution: generating short pulses of neutron

radiation. Spatial distribution of the neutron dose was measured by the dosimeter-radiometer.

The flux of the generated epithermal neutrons provides selective destruction of malignant tumor cells incubated in the boron-phenylalanine medium *in vitro*.

A new concept of the compact medical installation for BNCT is proposed. In this system, an orthogonal beam of neutrons is formed and a high-voltage power supply is placed inside the insulator of accelerator.

A new method of forming monoenergetic neutron flux is proposed, in which the dependence between the neutron energy and the angle of their emission from thin lithium layer in reaction ${}^7\text{Li}(p,n){}^7\text{Be}$ is used. The possibility of using this method for calibrating the detectors of weakly interacting particles is established.

Tandem accelerator with vacuum insulation and specialized targets makes it possible to carry out the generation of fast neutrons for neutron therapy and for dating rocks; monochromatic gamma-rays and resonance gamma-rays for the development of operational methods of detection of explosives and drugs; and α -particles for investigating promising neutronless thermonuclear fusion reaction ${}^{11}\text{B}(p,\alpha)\alpha\alpha$ and the positron generation.

ACKNOWLEDGMENTS

The work was supported by the International Science and Technology Center, Fund of Civilian Research and Development (US), Ministry of Education and Science of the Russian Federation, and Russian Science Foundation for Basic Research (project no. 14-32-00006) and BINP.

REFERENCES

1. G. L. Locher, "Biological effects and therapeutic possibilities of neutrons," *Am. J. Roentgenol. Radium Ther.* **36**, 1–13 (1936).
2. J. Chadwick, "The existence of a neutron," *Proc. R. Soc. (London)* **A136**, 692–708 (1932).
3. H. J. Taylor and M. Goldhaber, "Detection of nuclear disintegration in a photographic emulsion," *Nature (London)* **135**, 341–348 (1935).
4. P. G. Kruger, "Some biological effects of nuclear disintegration products on neoplastic tissue," *Proc. Natl. Acad. Sci. USA* **26**, 181–192 (1940).
5. W. H. Sweet, "The uses of nuclear disintegration in the diagnosis and treatment of brain tumor," *N. Engl. J. Med.* **245**, 875–878 (1951).
6. W. H. Sweet and M. Javid, "The possible use of slow neutrons plus boron-10 in the therapy of intracranial tumors," *Trans. Am. Neurol. Assoc.* **76**, 60–63 (1951).
7. *Neutron Capture Therapy. Principles and Applications*, Ed. by W. Sauerwein, A. Wittig, R. Moss, and Y. Nakagawa, (Springer, Berlin, 2012), p. 553.
8. L. E. Farr, W. H. Sweet, J. S. Robertson, C. G. Foster, H. B. Locksley, D. L. Sutherland, M. L. Mendelsohn, and E. E. Syckley, "Neutron capture therapy with boron in the treatment of glioblastoma multiforme," *Am. J. Roent.* **71**, 279–293 (1954).
9. J. T. Goldwin, L. E. Farr, W. H. Sweet, and J. S. Robertson, "Pathology study of eight patients with glioblastoma multiforme treated by neutron capture therapy using boron-10," *Cancer* **8**, 601–615 (1955).
10. D. N. Slatkin, "A history of boron neutron capture therapy of brain tumours," *Brain* **114**, 1609–1629 (1991).
11. W. Sauerwein, "Principles and history of neutron capture therapy," *Strahlenther Onkol.* **169**, 1–6 (1993).
12. A. Soloway, H. Hatanaka, and M. Davis, "Penetration of brain and brain tumor. 7. Tumor binding sulfhydryl boron compounds," *J. Med. Chem.* **10**, 714–717 (1967).
13. H. Hatanaka, "Clinical results of boron neutron capture therapy," *Basic Life Sci.* **54**, 15–21 (1990).
14. Y. Mishima, M. Ichihashi, S. Hatta, C. Honda, A. Sasase, K. Yamamura, K. Kenda, T. Kobayashi, and H. Fukuda, "Selective thermal neutron capture therapy and diagnosis of malignant melanoma: from basic studies to first clinical treatment," *Basic Life Sci.* **50**, 251–260 (1989).
15. A. Granada, J. Capala, M. Chadha, J. Codere, A. Diaz, A. Elowitz, I. Iwai, D. Joel, H. Liu, R. Ma, N. Pendzick, N. Peress, M. Shady, D. Slatkin, G. Tyson, and L. Wielopolski, "Boron neutron capture therapy for glioblastoma multiforme: interim results from the phase I/II dose-escalation studies," *J. Neurosurg.* **44** (6), 1182–1192 (1999).
16. P. Busse, O. Harling, M. Palmer, W. Kiger, III, J. Kaplan, I. Kaplan, C. Chuang, J. Goorley, K. Riley, T. Newton, A. Santa Cruz, X. Liu, and R. Zamenhof, "A critical examination of the results from the Harvard-MIT NCT program phase I clinical trials of neutron capture therapy for intracranial disease," *J. Neuro-Oncol.* **62** (1), 11–121 (2003).
17. W. Sauerwein and A. Zurlo, "The EORTC boron neutron capture therapy (BNCT) group: achievements and future projects," *Eur. J. Cancer* **38** (4), S31–S34 (2002).
18. H. Joensuu, L. Kankaanranta, T. Seppala, I. Auterinen, M. Kalio, M. Kulvik, J. Laakso, J. Vahatalo, M. Kortensniemi, P. Kotiluoto, T. Seren, J. Karila, A. Brander, E. Jarviluoma, P. Ryyanen, A. Pauteu, I. Ruokonen, H. Minn, M. Tenhunen, J. Jaaskelainen, M. Farkkila, and S. Savolainen, "Boron neutron capture therapy of brain tumors: clinical trials at the finish facility using boronophenylalanine," *J. Neuro-Oncol.* **62**, 123–134 (2003).
19. J. Capala, B. H. Stenstam, K. Skold, P. Rosenschold, V. Guisti, C. Persson, E. Wallin, A. Brum, L. Franzen, J. Carlsson, L. Salford, C. Ceberg, B. Persson, L. Pellettieri, and R. Heriksson, "Boron neutron capture therapy for glioblastoma multiforme: clinical studies in sweden," *J. Neuro-Oncol.* **62**, 135–144 (2003).
20. V. Dbaly, F. Tovarys, H. Honova, L. Petruzzelka, K. Prokes, J. Burian, M. Marek, J. Honzatko, I. Tomandl, O. Kriz, I. Janku, and V. Mares, "Contemporary state of neutron capture therapy in Czech

- Republic. (Part 2),” *Ces a Slov Neurol. Neurochir.* **66** (1), 60–63 (2002).
21. Y. Nakagawa, K. Pooh, T. Kobayashi, T. Kageji, S. Uyama, A. Matsumura, and H. Kumada, “Clinical review of the Japanese experience with boron neutron capture therapy and proposed strategy using epithermal neutron beams,” *J. Neuro-Oncol.* **62**, 87–99 (2003).
 22. S. J. Gonzalez, M. R. Bonomi, G. A. Santa Cruz, H. R. Blaumann, O. A. Larriou Calzetta, P. Menéndez, R. Jiménez Rebagliati, J. Longhino, D. B. Feld, M. A. Dagrosa, C. Argerich, S. G. Castiglia, D. A. Batistoni, S. J. Liberman, and B. M. C. Rothet, “First BNCT treatment of a skin melanoma in Argentina: dosimetric analysis and clinical outcome,” *Appl. Radiat. Isot.* **61** (5), 1101–1105 (2004).
 23. Y. W. Liu, T. T. Huang, S. H. Jiang, and H. M. Liu, “Renovation of epithermal neutron beam for BNCT at THOR,” *Appl. Radiat. Isot.* **61** (5), 1039–1043 (2004).
 24. I. Kato, K. Ono, Y. Sakurai, M. Ohmae, A. Maruhashi, Y. Imahori, M. Kirihata, M. Nakazawa, and Y. Yura, “Effectiveness of BNCT for recurrent head and neck malignancies,” *Appl. Radiat. Isot.* **61** (5), 1069–1073 (2004).
 25. L. Kankaanranta, T. Seppala, H. Koivunovo, K. Saariliagti, T. Atula, J. Collan, E. Salli, M. Kortensniemi, J. Simola, P. Valimaki, A. Makitie, M. Sappanen, H. Minn, H. Revitzer, M. Kouri, et al., “Boron neutron capture therapy in the treatment of locally recurred head and neck cancer: final analysis of a phase I/II trial,” *Int. J. Radiat. Oncol. Biol. Phys.* **82** (1), e67–e71 (2007).
 26. Y. Tamura, S. Miyatake, N. Nonogichi, S. Miyata, K. Yokoyama, T. Kuroiwa, M. Asada, H. Tanabe, and K. Ono, “Boron neutron capture therapy for recurrent malignant melanoma. Case report,” *J. Neurosurg.* **105** (6), 898–903 (2006).
 27. M. Suzuki, K. Endo, H. Satoh, Y. Sakurai, H. Kumada, H. Kimura, S. Masunaga, Y. Kinashi, K. Nagata, A. Maruhashi, and K. Ono, “A novel concept of treatment of diffuse or multiple pleural tumors by boron neutron capture therapy (BNCT),” *Radiother. Oncol.* **88** (2), 192–195 (2008).
 28. M. Suzuki, Y. Sakurai, S. Hagiwara, S. Masunaga, Y. Kinashi, K. Nagata, A. Maruhashi, M. Kudo, and K. Ono, “First attempt of boron neutron capture therapy (BNCT) for hepatocellular carcinoma,” *Jpn. J. Clin. Oncol.* **37** (5), 376–381 (2007).
 29. *Reference Tables of Physical Quantities*, Ed. by I. K. Kikoin (Atomizdat, Moscow, 1976) [in Russian].
 30. V. Kononov, M. Bokhovko, and O. Kononov, “Accelerator based neutron sources for medicine,” in *Proc. Int. Symp. on Boron Neutron Capture Therapy* (Novosibirsk, 2004), pp. 62–68.
 31. T. Blue and J. Yanch, “Accelerator-based epithermal neutron sources for boron neutron capture therapy of brain tumors,” *J. Neuro-Oncol.* **62**, 19–31 (2003).
 32. C. Lee and X. Zhou, “Thick target neutron yields for the ${}^7\text{Li}(p,n){}^7\text{Be}$ reaction near threshold,” *Nucl. Instrum. Meth. B* **152**, 1–11 (1999).
 33. K. Wang, T. Blue, and R. Gabauer, “A neutronic study of an accelerator-based neutron irradiation facility for boron neutron capture therapy,” *Nucl. Technol.* **84**, 93 (1989).
 34. J. Yanch, X. Zhou, R. Shefer, and R. Klinkowstein, “Accelerator-based epithermal neutron beam design for neutron capture therapy,” *Med. Phys.* **19**, 709–721 (1992).
 35. O. Anderson, E. Alpen, G. DeVries, J. Kwan, R. Wells, A. Faltens, and L. Reginato, “ESQ-focused 2.5 MeV dc accelerator for BNCT,” in *Proc. 4th Eur. Part. Accelerator Conf.* (London, 1994).
 36. *Advances in Neutron Capture Therapy, V. 1: Medicine and Physics*, Ed. by B. Larsson (Elsevier, 1997).
 37. J. L. Duggan, (Ed.) “Application of accelerators in research and industry,” *AIP Conf. Proc.* **392** (1997).
 38. *Proc. 1st Int. Workshop on Accelerator-based Neutron Sources for BNCT* (Jackson, WN, USA CONF-940976, 1994).
 39. J. Yanch, “Research in boron neutron capture therapy at MIT LABA,” *Application of Accelerators in Research and Industry. Part Two, 1281–1284. Woodbury*, Ed. by J. L. Duggan, I. L. Morgan (AIP Press, New York, 1996).
 40. D. P. Gierga, Ph.D. Thesis (Massachusetts Institute of Technology, 2001).
 41. J. Kwan, G. Ackerman, C. Chan, W. Cooper, G. Vries, W. Steele, M. Stuart, M. Vella, R. Wells, T. Inoue, Y. Okumura, and M. Mizuno, “Acceleration of 100 mA of H^- in a single channel electrostatic quadrupole accelerator,” *Rev. Sci. Instrum.* **66**, 3864–3868 (1995).
 42. B. Ludewigt, W. Chu, R. Donahue, J. Kwan, K. Leung, L. Reginato, and R. Wells, “An epithermal neutron source for BNCT based on an ESQ-accelerator,” in *Proc. Topical Meeting on Nuclear Applications of Accelerator Technology* (Albuquerque, New Mexico, 1997).
 43. T. P. Wangler, J. E. Stovall, T. S. Bhatia, et al., “Conceptual design of an RFQ accelerator-based neutron source for boron neutron capture therapy,” *Los Alamos National Laboratory article LAUR89-912, 1989: Particle Accelerator Conf.* (Chicago, IL, 1989).
 44. W. D. Cornelius, “CW operation of the FMIT RFQ accelerator,” *Nucl. Instrum. Meth. Phys. Res. B* **10–11**, 859–863 (1985).
 45. G. E. McMichael, T. J. Yule, and X.-L. Zhou, “The argon ACWL, a potential accelerator-based neutron source for BNCT,” *Nucl. Instrum. Meth. Phys. Res. B* **99** (1–4), 847–850 (1995).
 46. T. Beynon, K. S. Forcey, S. Green, G. Cruickshank, and N. James, “Status of the Birmingham accelerator based BNCT facility,” *Research and Development in Neutron Capture Therapy*, Sauerwein M.W., Moss R., Wittig A. (Eds.) (Bologna: Monduzzi Editore, Intern. Proc. Division, 2002), pp. 225–228.
 47. B. I. Al’bertinskii, I. V. Kuritsyna, O. F. Nikolaev, and O. B. Ovchinnikov, “High-voltage supply for 2 MeV accelerators of ions and electrons,” *Prib. Tekh. Eksper.* **3**, 43–46 (1971) [in Russian].
 48. A. Kreiner, H. Paolo, A. Burton, J. Kesque, A. Vakda, M. Debray, Y. Giboudot, P. Levinas, M. Fraiman,

- V. Romeo, H. Somacal, and D. Minsky, "Development of a tandem-electrostatic-quadrupole for accelerator-based boron neutron capture therapy," in *Proc. 8th Intern. Topical Meeting on Nuclear Applications and Utilization of Accelerators* (Pocatello, Idaho, 2007), pp. 373–379.
49. A. Kreiner, V. Vento, P. Levinas, J. Bergueiro, H. Di Paolo, A. Burlon, J. Kesque, A. Valda, M. Debray, H. Somacal, D. Minsky, L. Estrada, A. Hazarabedian, F. Johann, J. Sandin Suarez, et al., "Development of a tandem-electrostatic-quadrupole accelerator facility for BNCT," *Appl. Radiat. Isot.* **67**, S266–S269 (2009).
 50. J. Esposito, P. Colautti, A. Pisent, L. Tecchio, S. Agosto, Sanchez C. Ceballos, V. Conte, L. De Nardo, A. Gervash, R. Giniyatulin, D. Moro, A. Makhankov, I. Mazul, G. Rosi, et al., "The accelerator driven SPES-BNCT project at INFN Legnaro LABS," in *Proc. 8th Intern. Topical Meeting on Nuclear Applications and Utilization of Accelerators* (Pocatello, Idaho, 2007), pp. 380–387.
 51. J. Esposito, P. Colautti, S. Fabritsiev, A. Gervash, R. Giniyatulin, V. N. Lomasov, A. Makhankov, I. Mazul, A. Pisent, A. Pokrovsky, M. Rumyantsev, V. Tanchuk, and L. Tecchio, "Be target development for the accelerator-based SPES-BNCT facility at INFN Legnaro," *Appl. Radiat. Isot.* **67**, S270–S273 (2009).
 52. T. Smick, G. Ryding, P. Farrell, N. Smick, W. Oark, P. Eide, T. Sakase, M. Venkatesan, and M. Vyvoda, "Hyperion™ accelerator technology for boron neutron capture therapy," in *Book of Abstr. 16th Int. Cong. on Neutron Capture Therapy* (Finland, Helsinki, 2014), 138–139.
 53. E. Forton, F. Stichelbaut, A. Cambriani, W. Kleeven, J. Ahlback, and Y. Jongen, "Overview of the IBA accelerator-based BNCT system," *Appl. Rad. Isot.* **67** (7–8), S262–S268 (2009).
 54. K. Tsuchida, Y. Kiyanagi, A. Uritani, K. Watanabe, H. Shimizu, K. Hirota, and M. Kitaguchi, "Development of an accelerator-driven compact neutron source for BNCT in Nagoya University," in *Book of Abstr. 16th Int. Cong. on Neutron Capture Therapy* (Finland, Helsinki, 2014), 206–207.
 55. Y. Mori and M. Muto, "Neutron source with FFAG-ERIT," in *Advances in Neutron Capture Therapy* (Proc. ICNCT-12, 2006), pp. 360–363.
 56. K. Okabe, M. Muto, and Y. Mori, "Development of FFAG-ERIT ring," in *Proc. EPAC* (Edinburgh, Scotland, 2006), pp. 1675–1677.
 57. Y. Mori, Y. Ishi, Y. Kuriyama, Y. Sakurai, T. Uesugi, K. Okabe, and I. Sakai, "Neutron source with emittance recovery internal target," in *Proc. 23rd Particle Accelerator Conf.* (Vancouver, Canada, 2009), pp. 3145–3147.
 58. H. Tanaka, Y. Sakurai, M. Suzuki, T. Takata, S. Masunaga, Y. Kinashi, G. Kashino, Y. Liu, T. Mitsumoto, T. Yajima, H. Tsutsui, M. Takada, A. Maruhashi, and K. Ono, "Improvement of dose distribution in phantom by using epithermal neutron source based on the Be(p,n) reaction using a 30 MeV proton cyclotron," *Appl. Radiat. Isot.* **67** (7/8) S258–S261 (2009).
 59. H. Tanaka, Y. Sakurai, M. Suzuki, S. Masunaga, T. Mitsumoto, K. Fujita, G. Kashino, Y. Kinashi, Y. Liu, M. Takada, K. Ono, and A. Maruhashi, "Experimental verification of beam characteristics for cyclotron-based epithermal neutron source (C-BENS)," *Appl. Radiat. Isot.* **69** (12) 1642–1645 (2011).
 60. H. Kumada, A. Matsumura, H. Sakurai, T. Sakae, M. Yoshioka, H. Kobayashi, H. Matsumoyo, Y. Kijanagi, T. Shibata, and H. Nakashima, "Project of development of the linac based NCT facility in University of Tsukuba," in *Abstr. 15th ICNCT* (Tsukuba, Japan, 2012) p. 109.
 61. Y. Abe, M. Fuse, R. Fujii, M. Nakamura, Y. Imahori, J. Itami, "Hospital-based boron neutron capture therapy in National Cancer Center. An installation design for the accelerator-based epithermal neutron source," in *Abstr. 15th ICNCT* (Tsukuba, Japan, 2012), pp. 109–110.
 62. B. Bayanov, V. Belov, E. Bender, M. Bokhovko, G. Dimov, V. Kononov, O. Kononov, N. Kuksanov, V. Palchikov, V. Pivovarov, R. Salimov, G. Silvestrov, A. Skrinky, and S. Taskaev, "Accelerator based neutron source for the neutron-capture and fast neutron therapy at hospital," *Nucl. Instrum. Meth. Phys. Res. A* **413** (2/3), 397–426 (1998).
 63. Yu. I. Bel'chenko, A. V. Burdakov, V. I. Davydenko, V. M. Dolgushin, A. N. Dranichnikov, A. A. Ivanov, V. V. Kobets, S. G. Konstantinov, A. S. Krivenko, A. M. Kudryavtsev, V. Ya. Savkin, A. L. Sanin, I. N. Sorokin, S. Yu. Taskaev, M. A. Tiunov, A. D. Khilchenko, and V. V. Shirokov, "Tandem accelerator with vacuum isolation as the base for medical complex for treating malignant tumors by using BNCT and customs system for remote detection of explosives," *Vestn. NGU: Ser. Fizika* **1** (2) 82–88 (2006).
 64. *Proceedings of International Symposium on Boron Neutron Capture Therapy*, Ed by S. Taskaev (Novosibirsk, Russia, 2004) p. 113.
 65. Y. Belchenko and E. Grigoryev, "Surface-plasma negative ion source for the medicine accelerator," *Rev. Sci. Instrum.* **73**, 939 (2002).
 66. Yu. Belchenko, A. Sanin, I. Gusev, A. Khilchenko, A. Kvashnin, V. Rashchenko, V. Savkin, and P. Zubarev, "Direct current H⁻ source for boron neutron capture therapy tandem accelerator," *Rev. Sci. Instrum.* **79**, 02A521 (2008).
 67. T. Akhmetov, V. Davydenko, A. Ivanov, V. Kobets, A. Medvedko, D. Skorobogatov, and M. Tiunov, "Radially uniform circular sweep of ion beam," *Rev. Sci. Instrum.* **77**, 03106 (2006).
 68. R. Salimov, V. Cherepkov, Yu. Golubenko, G. Krainov, M. Korabelnikov, S. Kuznetsov, N. Kuksanov, A. Malinin, P. Nemytov, S. Petrov, V. Prudnikov, S. Fadeev, and M. Veis, "DC high power electron accelerators of ELV-series: status, development, applications," *Rad. Phys. Chem.* **57**, 661–665 (2000).
 69. V. V. Shirokov, "Investigation of the electrical strength of high-voltage vacuum gaps," *Prib. Tekh. Eksper.* **5**, 148–152 (1990).
 70. G. I. Dimov, Yu. I. Bel'chenko, G. S. Krainov, R. A. Salimov, N. K. Kuksanov, G. I. Sil'vestrov, I. N. Sorokin, S. Yu. Taskaev, M. A. Tiunov, D. K. Toporkov, and V. V. Shirokov, "Tandem accel-

- ator with vacuum insulation for boron-neutron-capture therapy and detection of explosives by resonance absorption of γ -rays," *At. Energy* **94** (2), 155–159 (2003).
71. I. N. Sorokin and V. V. Shirokov, "High-voltage elements of a tandem accelerator with vacuum insulation," *Instrum. Exp. Tech.* **50**, 719–724 (2007).
 72. I. N. Sorokin and S. Yu. Taskaev, "A voltage buildup at high-voltage vacuum gaps of a tandem accelerator with vacuum insulation," *Instrum. Exp. Tech.* **57**, 377–380 (2014).
 73. V. I. Aleinik, A. A. Ivanov, A. S. Kuznetsov, I. N. Sorokin, and S. Yu. Taskaev, "Dark current of a tandem accelerator with vacuum insulation," *Instrum. Exp. Tech.* **56**, 497–505 (2013).
 74. I. N. Sorokin, "High-voltage strength of the tandem accelerator with vacuum insulation" Candidates's Dissertation in Mathematics and Physics (Novosibirsk, 2014).
 75. G. E. Derevyankin, G. S. Krainov, A. M. Kryuchkov, G. I. Sil'vestrov, S. Yu. Taskaev, and M. A. Tiunov, "Ion-optical tract of 2.5 MeV 10 mA tandem accelerator," Preprint IYaF 2002-24 (Novosibirsk, 2002).
 76. V. I. Aleinik, A. G. Bashkirtsev, A. S. Kuznetsov, A. N. Makarov, I. N. Sorokin, S. Yu. Taskaev, M. A. Tiunov, and I. M. Shchudlo, "Optimization of the transporting system of the negative hydrogen ions in tandem accelerator with vacuum insulation," *Dokl. Akad. Nauk Vyssh. Shkoly RF* **20** (1), 47–55 (2013).
 77. A. Makarov, V. Aleynik, A. Bashkirtsev, A. Kuznetsov, I. Shchudlo, I. Sorokin, S. Taskaev, and M. Tiunov, "Optimization of the negative hydrogen ion beam injection into the tandem accelerator with vacuum insulation," in *Proc. 23 Russian Particle Accelerator Conference, RUPAC2012* (St.-Petersburg, 2012), pp. 623–625.
 78. G. E. Derevyankin, G. I. Dimov, V. M. Dolgushin, A. N. Dranichnikov, G. S. Krainov, A. S. Krivenko, V. E. Pal'chikov, M. V. Petrichenkov, E. I. Pokhlebin, R. A. Salimov, G. I. Sil'vestrov, S. Yu. Taskaev, and V. V. Shirokov, "Rechargeable target of a 40 mA 2 MeV tandem accelerator," Preprint No. IYaF 2001-23 (Novosibirsk, 2001).
 79. V. I. Aleinik, A. S. Kuznetsov, I. N. Sorokin, S. Yu. Taskaev, M. A. Tiunov, and I. M. Shchudlo, "Calibration of the stripping target of a tandem accelerator with vacuum insulation," *Nauch. Vestn. Novosibirsk Gos. Tekh. Univ.* **50** (1), 83–92 (2013).
 80. A. Kuznetsov, V. Aleynik, I. Shchudlo, I. Sorokin, S. Taskaev, and M. Tiunov, "Calibration testing of the stripping target of the vacuum insulated tandem accelerator," in *Proc. 23 Russian Particle Accelerator Conference, RUPAC2012* (Saint-Petersburg, Russia, 2012), pp. 560–562.
 81. A. S. Kuznetsov, G. N. Malyshev, A. N. Makarov, I. N. Sorokin, Yu. S. Sulyaev, and S. Yu. Taskaev, "First experiments on neutron detection on the accelerator-based source for boron neutron capture therapy," *Tech. Phys. Lett.* **35** (4) 346–348 (2009).
 82. A. Kuznetsov, Yu. Belchenko, A. Burdakov, V. Davydenko, A. Donin, A. Ivanov, S. Konstantinov, A. Krivenko, A. Kudryavtsev, K. Mekler, A. Sanin, I. Sorokin, Yu. Sulyaev, S. Taskaev, V. Shirokov and Yu. Eidelman, "The detection of nitrogen using nuclear resonance absorption of mono-energetic gamma-rays," *Nucl. Instrum. Meth. Phys. Res. A* **606**, 238–242 (2009).
 83. D. Kasatov, A. Kuznetsov, A. Makarov, I. Shchudlo, I. Sorokin, and S. Taskaev, "Proton beam of 2 MeV 1.6 mA on a tandem accelerator with vacuum insulation," *JINST* **9**, 12016 (2014).
 84. W. Biesiot and P. Smith, "Parameters of the 9.17-MeV level in ^{14}N ," *Phys. Rev. C* **24**, 2443–2457 (1981).
 85. V. I. Aleinik, D. A. Kasatov, A. N. Makarov, and S. Yu. Taskaev, "Measuring the neutron spectrum of the accelerator-based source using the time-of-flight method," *Instrum. Exp. Tech.* **57** 381–385 (2014).
 86. D. A. Kasatov, A. N. Makarov, S. Yu. Taskaev, and I. M. Shchudlo, "Recording of current accompanying an ion beam in a tandem accelerator with vacuum insulation," *Tech. Phys. Lett.* **41** (92) 139–141 (2015).
 87. S. Yu. Taskaev, RF Patent No. 2013140568 (2013).
 88. V. Belov, S. Fadeev, V. Karasyuk, V. Kononov, O. Kononov, N. Kuksanov, G. Kraynov, Y. Petrov, V. Pidiyakov, V. Rachkov, R. Salimov, G. Silvestrov, G. Smirnov, S. Taskaev, and G. Villeval'd, "Neutron producing target for accelerator based neutron source for BNCT," *Research and Development in Neutron Capture Therapy* (Monduzzi Editore, 2002), pp. 247–252.
 89. G. G. Smirnov, S. Yu. Taskaev, G. I. Sil'vestrov, and V. N. Kononov, RF Patent No. 2282908 (2006).
 90. G. G. Smirnov, S. Yu. Taskaev, G. I. Sil'vestrov, and V. N. Kononov, RF Patent No. 2282909 (2006).
 91. G. G. Smirnov, S. Yu. Taskaev, G. I. Sil'vestrov, and V. N. Kononov, RF Patent No. 2326513 (2008).
 92. V. Kononov, G. Smirnov, and S. Taskaev, "Tape high power neutron producing target for NCT," in *Program 11th World Cong. on Neutron Capture Therapy* (MA, USA, Boston, 2004), pp. 46–47.
 93. B. Bayanov, V. Belov, and S. Taskaev, "Neutron producing target for accelerator based neutron capture therapy," *J. Phys.* **41**, 460–465 (2006).
 94. V. Belov, S. Fadeev, V. Karasyuk, V. Kononov, O. Kononov, A. Krivenko, N. Markov, V. Palchikov, G. Silvestrov, G. Smirnov, and S. Taskaev, "Neutron producing target for neutron capture therapy," in *Proc. 9th Int. Symp. on Neutron Capture Therapy for Cancer* (Osaka, Japan, 2000), pp. 253–254.
 95. O. E. Kononov, V. N. Kononov, and N. A. Solov'ev, "Near-threshold $^7\text{Li}(p,n)^7\text{Be}$ reaction based neutron source for boron neutron capture therapy," *Atomic Energy* **94**, 469–472 (2003).
 96. B. F. Bayanov, V. P. Belov, and S. Yu. Taskaev, "Neutron-generating target of accelerator neutron source for neutron capture therapy," Preprint IYaF 2005-4 (Novosibirsk, 2005).
 97. B. Bayanov, V. Belov, V. Kindyuk, E. Oparin, and S. Taskaev, "Lithium neutron producing target for BINP accelerator-based neutron source," *Appl. Radiat. Isot.* **61**, 817–821 (2004).
 98. H. Andersen and J. Ziegler, *Hydrogen Stopping Powers and Ranges in all Elements. Vol. 3* (Pergamon, N. Y., 1977).

99. N. Cowern, "Range distribution function for energetic ions in matter," *Phys. Rev. A* **26**, 2518–2526 (1982).
100. *Sputtering by Particle Bombardment*, Ed by R. Berish (Springer, Berlin, 1981).
101. M. I. Guseva and Yu. V. Martynenko, "Radiation blistering," *Sov. Phys. Usp.* **24**, 996–1007 (1981).
102. D. Fisher, *Hydrogen Diffusion in Metals, a 30-Year Retrospective* (Scitech Publ., 1999).
103. *Gase und Kohlenstoff in Metallen*, Ed. by E. Fromm and E. Gebhardt (Springer, Berlin, 1976).
104. V. Astrelin, A. Burdakov, P. Bykov, I. Ivanov, A. Ivanov, Y. Jongen, S. Konstantinov, A. Kudryavtsev, K. Kuklin, K. Mekler, S. Polosatkin, V. Postupaev, A. Rovenskiikh, S. Sinitskiy, and E. Zubairov, "Blistering of the selected materials irradiated by intense 200 keV proton beam," *J. Nucl. Mater.* **396**, 43–48 (2010).
105. R. Yadava, Singh N. Ibobi, and A. Nigam, "Sponge-like blisters on copper by H⁺ ion implantation at ambient temperatures," *J. Phys. D: Appl. Phys.* **13**, 2077–2080 (1980).
106. S. Melnychuk and R. Meilunas, "Development of a thin film 9.17 MeV gamma ray production target for the contraband detection system," in *Proc. Particle Accelerator Conference* (New York, 1999), pp. 2599–2601.
107. V. N. Kononov, M. V. Bokhovko, O. E. Kononov, and N. P. Kononova, "Gamma-radiation of ⁷Li(p,n)⁷Be neutron source," Preprint FEI-2643 (Obninsk, 1997).
108. A. Savidou, X. Aslanoglou, T. Paradellis, and M. Pila-kouta, "Proton induced thick target γ -ray yields of light nuclei at the energy region $E_p = 1.0$ – 4.1 MeV," *Nucl. Instrum. Meth. Phys. Res. B* **152** (1999).
109. J. Farrell, V. Dudnikov, N. Guardala, G. Merkel, and S. Taskaev, "An intense positron beam source based on a high current 2 MeV vacuum insulated tandem accelerator," in *7th Int. Workshop on Positron and Positronium Chemistry* (Knoxville, USA, 2002), p. 47.
110. D. A. Kasatov, A. N. Makarov, S. Yu. Taskaev, and I. M. Shchudlo, "Radiation due to absorption of 2 MeV protons in different materials," *Phys. At. Nucl.* (2015) (in press, vol. 78, no. 11).
111. B. F. Bayanov and S. Yu. Taskaev, RF Patent No. WO/2008/147230 (2008).
112. B. F. Bayanov, E. V. Zhurov, and S. Yu. Taskaev, "Measuring the lithium layer thickness," *Instrum. Exp. Tech.* **51** 147–149 (2008).
113. A. Brown, K. Forsey, and M. Scott, "The design and testing high power lithium target for accelerator-based boron neutron capture therapy," *Research and Development in Neutron Capture Therapy* (Monduzzi Editore, 2002), pp. 277–282.
114. B. F. Bayanov, S. Yu. Taskaev, V. I. Obodnikov, and E. G. Tishkovskii, "Effect of the residual gas on the lithium layer of a neutron-generating target," *Instrum. Exp. Tech.* **51**, 438–442 (2008).
115. Ya. Z. Kandiev and E. V. Serova, "Tagged particles in radiation transport using the Monte Carlo simulation and computer program PRIZMA," *At. Energy* **98**, 386–393 (2005).
116. *Schemes of Radionuclide Decay. Energy and Intensity of Radiation* (Energoatomizdat, Moscow, 1987) [in Russian].
117. V. P. Mashkovich and A. V. Kudryavtseva, *Protection Against Ionizing Radiation. Reference Book* (Energoatomizdat, Moscow, 1995) [in Russian].
118. *Basic Sanitary Rules for Radiation Safety (OSPORB-99)* (Minzdrav Rossii, Moscow, 2000) [in Russian].
119. B. F. Bayanov, Ya. Z. Kandiev, E. A. Kashaeva, G. N. Malyshkin, S. Yu. Taskaev, V. Ya. Chudaev, "A protective subsurface container for holding and temporary storage of activated targets," *Instrum. Exp. Tech.* **53** (6), 883–885 (2010).
120. S. Taskaev, B. Bayanov, V. Belov, and E. Zhoorov, "Development of lithium target for accelerator based neutron capture therapy," in *Adv. Neutron Capture Ther.* (Proc. ICNT-12, 2006), pp. 292–295.
121. T. Mitsumoto, S. Yajiima, H. Tsutsui, et al., "Cyclotron-based neutron source for BNCT" in *Proc. 14 Int Cong. on Neutron Capture Therapy* (Argentina, Buenos Aires, 2010), pp. 510–522.
122. C. Willis, J. Lenz, and D. Swenson, "High-power lithium target for accelerator-based BNCT," in *Proc. 14 Linear Accelerator Conf.* (Victoria, Canada, 2008), pp. 223–225.
123. S. Park, H. Joo, B. Jang, G. Jeun, J. Kim, and J. Chai, "Thermally optimized lithium neutron producing target design for accelerator-based BNCT," in *Advances in Neutron Capture Therapy* (Proc. ICNCT-12, 2006), pp. 319–322.
124. F. Palamara, F. Mattioda, R. Varone, and V. Guisti, "Proton accelerator-based epithermal neutron beams for BNCT," *Research and Development in Neutron Capture Therapy* (Monduzzi Editore, 2002), pp. 283–292.
125. A. Hawk, T. Blue, J. Woolard, and G. Gupta, "Effects of target thickness on neutron field quality for an ABNS," *Research and Development in Neutron Capture Therapy* (Monduzzi Editore, 2002), pp. 253–257.
126. O. Kononov, V. Kononov, M. Bokhovko, V. Korobeynikov, A. Soloviev, A. Sysyov, I. Gulidov, W. Chu, and D. Nigg, "Optimization of an accelerator-based neutron source for neutron capture therapy," *Appl. Radiat. Isot.* **61** (5), 1009–1011 (2004).
127. G. Bengua, T. Kobayashi, K. Tanaka, and Y. Nakagawa, "Optimization parameters for BDE in BNCT using near threshold ⁷Li(p,n)⁷Be direct neutrons," *Appl. Rad. Isot.* **61** (5), 1003–1008 (2004).
128. F. Stichelbaut, E. Forton, and Y. Jongen, "Design of a beam shaping assembly for an accelerator-based BNCT system," in *Adv. Neutron Capture Ther.* (Proc. ICNT-12, 2006), pp. 308–311.
129. K. Tanaka, T. Kobayashi, G. Bengua, Y. Nakagawa, S. Endo, and M. Hoshi, "Characterization indexes of moderator assembly for accelerator-based BNCT using ⁷Li(p,n)⁷Be neutrons at proton energy of 2.5 MeV," in *Adv. Neutron Capture Ther.* (Proc. ICNT-12, 2006), pp. 323–326.
130. R. Terlizzi, N. Colonna, P. Colangelo, A. Maiorana, S. Marrone, A. Rainò, G. Tagliente, and V. Variale, "Design of an accelerator-based neutron source for

- neutron capture therapy,” *Appl. Radiat. Isot.* **67** (7–8), S292–S295 (2009).
131. D. Minsky, A. Kreiner, and A. Valda, “AB-BNCT beam shaping assembly based on ${}^7\text{Li}(p,n){}^7\text{Be}$ reaction optimization,” *Appl. Radiat. Isot.* **69** (12), 1668–1671 (2011).
 132. A. Burlon, S. Girola, A. Valda, D. Minsky, A. Kreiner, and D. Sánchez, “Design of a beam shaping assembly and preliminary modeling of a treatment room for accelerator-based BNCT at CNEA,” *Appl. Radiat. Isot.* **69** (12), 1688–1691 (2011).
 133. J. Goorley, W. Kiger, III, and R. Zamenhof, “Reference dosimetry calculations for neutron capture therapy with comparison of analytical and voxel models,” *Med. Phys.* **29**, 145–156 (2002).
 134. O. Harling and K. Riley, “Fission reactor neutron sources for neutron capture therapy—a critical review,” *J. Neuro-Oncol.* **62**, 7–17 (2003).
 135. M. Arnautova, Ya. Kandiev, D. Lukhminsky, and G. Malyshkin, “Monte Carlo simulation in nuclear geophysics: comparison of the PRIZMA Monte Carlo program and benchmark experiments,” *Nucl. Geophys.* **7**, 407–418 (1993).
 136. S. N. Abramovich, B. Ya. Guzhovskii, V. A. Zherebtsov, and A. G. Zvenigiridskii, *Nuclear Constants for Thermonuclear Fusion* (Moscow, Tsentr. Nauch. Issled. Inst. Atominform, 1989) [in Russian].
 137. O. Kononov, V. Kononov, V. Korobeinikov, S. Ognev, W. Chu, G. Silvestrov, N. Soloviev, S. Taskaev, and A. Zhitnik, “Investigations of using near-threshold ${}^7\text{Li}(p,n){}^7\text{Be}$ reaction for NCT based on in-phantom dose distribution,” *Research and Development in Neutron Capture Therapy* (Monduzzi Editore, 2002), pp. 241–246.
 138. G. Bengua, T. Kobayashi, and K. Tanaka, “TPD-based evaluation of near threshold mono-energetic proton energies for the ${}^7\text{Li}(p,n){}^7\text{Be}$ production of neutrons for BNCT,” *Phys. Med. Biol.* **51**, 4095–4109 (2006).
 139. Ya. Kandiev, E. Kashaeva, G. Malyshkin, B. Bayanov, and S. Taskaev, “Optimization of the target of an accelerator-driven neutron source through Monte Carlo numerical simulation of neutron and gamma transport by the PRIZMA code,” *Appl. Radiat. Isot.* **69** (12), 1632–1634 (2011).
 140. S. Yu. Taskaev and V. V. Kanygin, RF Patent No. 2540124 (2014).
 141. B. Bayanov, A. Burdakov, V. Chudaev, A. Ivanov, S. Konstantinov, A. Kuznetsov, A. Makarov, G. Malyshkin, K. Mekler, I. Sorokin, Yu. Sulyaev, and S. Taskaev, “First neutron generation in the BINP accelerator based neutron source,” *Appl. Radiat. Isot.* **67** (7–8), S285–S287 (2009).
 142. V. Aleynik, B. Bayanov, A. Burdakov, A. Makarov, S. Sinitskiy, and S. Taskaev, “New technical solution for using the time-of-flight technique to measure neutron spectra,” *Appl. Radiat. Isot.* **69** (12), 1339–1641 (2011).
 143. V. Aleynik, A. Burdakov, V. Davydenko, A. Ivanov, V. Kanygin, A. Kuznetsov, A. Makarov, I. Sorokin, and S. Taskaev, “BINP accelerator based epithermal neutron source,” *Appl. Radiat. Isot.* **69** (12), 1635–1638 (2011).
 144. B. Bayanov, E. Kashaeva, A. Makarov, G. Malyshkin, S. Samarin, S. Taskaev, “A neutron producing target for BINP accelerator-based neutron source,” *Appl. Radiat. Isot.* **67** (7–8), S282–S284 (2009).
 145. B. Bayanov, A. Burdakov, A. Kuznetsov, A. Makarov, S. Sinitskii, Yu. Sulyaev, and S. Taskaev, “Dosimetry and spectrometry at accelerator based neutron source for boron neutron capture therapy,” *Radiat. Meas.* **45** (10), 1462–1464 (2010).
 146. A. V. Sannikov, V. N. Lebedev, V. N. Kustarev, E. N. Savitskaya, and E. G. Spirov, “Individual dosimeter of mixed radiation DVGN-1: development and investigation of characteristics,” Preprint IFVE 2005-6 (Protvino, 2005).
 147. A. G. Alekseev, Yu. V. Mokrov, and S. V. Morozova, “An investigation of the sensitivity of various albedo neutron dosimeters aimed at corrections the readings,” *Phys. Part. Nucl. Lett.* **9** (2), 192–201 (2012).
 148. L. A. Mostovich, N. V. Gubanov, O. S. Kutsenko, V. I. Aleinik, A. S. Kuznetsov, A. N. Makarov, I. N. Sorokin, S. Yu. Taskaev, G. I. Nepomnyashchikh, and E. V. Grigor’eva, “Impact of epithermal neutrons on the survivability of malignant cells of glioblastoma in vitro,” *Bull. Exper. Biol. Medicine* **151** (2), 229–235 (2011).
 149. N. Gubanov, V. Kanygin, A. Kichigin, and S. Taskaev, “Evaluation of micronucleation and viability of glioma cells in vitro neutron beams irradiated,” submitted for publication to *Appl. Radiat. Isot.* (2015).
 150. V. Aleynik, A. Bashkirtsev, V. Kanygin, D. Kasatov, A. Kuznetsov, A. Makarov, I. Schudlo, I. Sorokin, S. Taskaev, and M. Tiunov, “Current progress and future prospects of the VITA based neutron source,” *Appl. Radiat. Isot.* **88**, 177–179 (2014).
 151. I. Sorokin and S. Taskaev, “A new concept of a vacuum insulation tandem accelerator,” *Appl. Radiat. Isot.* (2015) (in press, DOI: 10.1016/j.apradiso.2015.06.015).
 152. I. N. Sorokin and S. Yu. Taskaev, RF Patent No. 2014139866 (2014).
 153. Y. Sofue and V. Rubin, “Rotation curves of spiral galaxies,” *Ann. Rev. Astron. Astrophys.* **39**, 137–174 (2001).
 154. R. Cabanac, D. Valls-Gabaud, A. Jaunsen, C. Lidman, and H. Jerjen, “Discovery of a high-redshift Einstein ring,” *Astron. Astrophys.* **436** (2), L21–L25 (2005).
 155. D. Spergel, R. Bean, O. Doré, M. Nolta, C. Bennett, J. Dunkley, G. Hinshaw, N. Jarosik, E. Komatsu, L. Page, H. Peiris, L. Verde, M. Halpern, R. Hill, A. Kogut, et al., “Wilkinson microwave anisotropy probe (WMAP) three year results: implications for cosmology,” *Astrophys. J. Suppl.* **170** (2), 377–408 (2007).
 156. S. Burles, K. Nollett, and M. Turner, “Big Bang nucleosynthesis predictions for precision cosmology,” *Astrophys. J.* **1**, L1–L5 (2001).
 157. N. Spooner, “Direct dark matter searches,” *J. Phys. Soc. Jpn.* **76**, 111016 (2007).
 158. R. Bernabei, P. Belli, A. Bussolotti, F. Cappella, R. Cerulli, C. Dai, A. d’Angelo, A. Incicchitti,

- H. Kuang, J. Ma, A. Mattei, F. Montecchia, F. Nozoli, D. Prosperi, X. Sheng, and Z. Ye, "The DAMA/LIBRA apparatus," *Nucl. Instrum. Meth. A* **592** (3), 297–315 (2008).
159. J. Angle, E. Aprile, and F. Arneodo, et al. (XENON Collaboration), "First results from the XENON10 dark matter experiment at the Gran Sasso National Laboratory," *Phys. Rev. Lett.* **100**, 021303 (2008).
160. M. Felizardo, T. Giraldo, T. Morlat, A. Fernandes, A. Ramos, and J. Marques, "Recent results from the SIMPLE dark matter search," *J. Phys.: Conf. Ser.* **375**, 012011 (2012).
161. H. Harano, T. Matsumoto, Y. Tanimura, Y. Shikaze, M. Baba, and T. Nakamura, "Monoenergetic and quasi-monoenergetic neutron reference fields in Japan," *Radiat. Meas.* **45** (10), 1076–1082 (2010).
162. V. Lacoste, "Review of radiation sources, calibration facilities and simulated workplace fields," *Radiat. Meas.* **45** (10), 1083–1089 (2010).
163. T. Matsumoto, H. Harano, J. Nishiyama, A. Uritani, and K. Kudo, "Novel generation method of 24-keV monoenergetic neutrons using accelerators," in *AIP Conf. Proc.*, **1099**, 924–927 (2009).
164. S. Yu. Taskaev, RF Patent No. 2515523 (2014).
165. A. N. Makarov and S. Yu. Taskaev, "Monoenergetic neutron beam for calibrating dark matter detectors," *JETP Lett.* **97** (12), 668–669 (2013).
166. A. E. Bondar', A. F. Buzulutskov, A. V. Burdakov, E. S. Grishnyaev, A. D. Dolgov, A. N. Makarov, S. V. Polosatkin, A. V. Sokolov, S. Yu. Taskaev, and L. I. Shekhtman, "Project of the systems of neutron scattering for calibration of the dark matter detectors and low-energy neutrinos," *Vestn. Novosibirsk Gosud. Universitet, Ser. Fiz.* **8** (3), 27–38 (2013).
167. M. L. E. Oliphant and Lord M. O. Rutherford, "Experiments on the transmutation of elements by protons," *Proc. R. Soc. A (London)* **141**, 259–281 (1933).
168. P. Dee and C. Gilbert, "The disintegration of boron into three α -particles," *Proc. R. Soc. A (London)* **154**, 279–296 (1936).
169. N. Rostoker, A. Qerushi, and M. Rinderbauer, "Colliding beam fusion reactors," *J. Fusion Energy* **22**, 83–92 (2004).
170. S. Stave, M. Ahmed, R. France, III, S. Henshaw, B. Muller, B. Perdue, R. Prior, M. Spraker, and H. Weller, "Understanding the $^{11}\text{B}(p,\alpha)\alpha$ reaction at the 0.675 MeV resonance," *Phys. Lett. B* **696**, 26–29 (2011).
171. V. Volosov, "Aneutronic fusion on the base of asymmetrical centrifugal trap," *Nucl. Fusion* **46**, 820–828 (2006).
172. V. Dmitriev, " α -Particle spectrum in the reaction $p + ^{11}\text{B} \rightarrow \alpha + ^8\text{Be}^* \rightarrow 3\alpha$," *Phys. Atom. Nucl.* **72** (7), 1165–1167 (2009).
173. H. Becker, C. Rolfs, and H. Trautvetter, "Low-energy cross sections for $^{11}\text{B}(p,3\alpha)^*$," *Z. Phys. A* **327**, 341–355 (1987).
174. J. Quebert and L. Marquez, "Effets des résonances de ^{12}C sur l'émission de particules alpha dans la réaction $^{11}\text{B}(p,3\alpha)$," *Nucl. Phys. A* **126**, 646–670 (1969).

Translated by G. Dedkov